Proceedings of the 1st Workshop on Phenomenology for Particle and Anti-Particle 2018 (PPAP2018)

6th-8th March 2018 , Graduate School of Science, Hiroshima University

Editors:
Takuya Morozumi[(a∗)],Hiroki Sakamoto [(a∗Webpage)], Yusuke Shimizu[(a∗)], Kenta Takagi[(a)], Shunya Takahashi[(a)]

Authors:
Kento Asai[(b)], Gabriela Barenboim[(c)],Pyungwon Ko[(d)], Kensuke Homma[(a)], Keiko Nagao[(e)], Apriadi Salim Adam[(a)], Kenta Takagi[(a)], Morimitsu Tanimoto[(f)], Kazushige Ueda[(a)], Masato Yamanaka[(g)],Norimi Yokozaki[(h)]

[∗] organizers, [a]*Hiroshima University*, [b]*Univ. of Tokyo*, [c]*Valencia, IFIC*, [d]*Korea Institute for Advanced Study*, [e]*National Institute of Technology, Niihama College, Okayama University of Science*, [f]*Niigata University*, [g]Maskawa Institute, Kyoto Sangyo University,[h]*Tohoku University*

Abstract

This is a proceedings for PPAP 2018. Thanks to speakers and participants, the workshop was timely and lively. The topics include Physics of Dark Matter, neutrinos and anti-neutrinos asymmetry, Non-abelian discrete symmetry as flavor symmetry, seesaw and CP violation, leptogenesis with gauged lepton number, search for Pseudo Nambu-Goldstone boson, particle number asymmetry, quantum entanglement , axion in hidden U(1), and CPT violation in neutrinos.

1 Program

	March 6 (Tue.)	
13:55-14:00	Opening	
14:00-16:00	Chairman : Morimitsu Tanimoto (Niigata University)	
14:00-15:00	Pyungwon Ko (Korea Institute for Advanced Study)	Dark pion DM : WIMP vs SIMP
15:00-15:15	Break	
15:15-16:00	Keiko Nagao (National Institute of Technology, Niihama College)	Anisotropy of dark matter velocity distribution
16:00-17:25	Chairman : Masato Yamanaka (Maskawa InstituteKyoto Sangyo University)	
16:00-16:30	Kazushige Ueda (Hiroshima University)	Research on Quantum Entanglement of the Vacuum of Fields
16:30-16:45	Break	
16:45-17:25	Apriadi Salim Adam (Hiroshima University)	Generation of particle number asymmetry in an expanding universe; a novel mechanism
	March 7 (Wed.)	
10:00-12:00	Chairman : Yusuke Shimizu (Hiroshima University)	
10:00-11:00	Gabriela Barenboim (Valencia, IFIC)	Flavor versus mass eigenstates in neutrino asymmetries: implications
11:00-11:15	Break	
11:15-12:00	Morimitsu Tanimoto (Niigata University)	Non-Abelian Discrete Groups and Neutrino Flavor Symmetry
12:00-14:00	Lunch	
14:00-16:30	Chairman : Keiko Nagao (National Institute of Technology, Niihama College)	
14:00-14:45	Kensuke Homma (Hiroshima University)	Searches for pseudo Nambu-Goldstone bosons by stimulated resonant photon-photon scatterings with high-intensity laser fields.
14:15-15:00	Break	
15:00-15:40	Masato Yamanaka (Maskawa Institute Kyoto Sangyo University)	Relation of CLFV to cosmological observables in the CMSSM coannihilation scenario with the seesaw mechanism
15:50-16:30	Kenta Takagi (Hiroshima University)	Towards the minimal seesaw model for the prediction of neutrino CP violation.
18:00-19:30	Dinner (Place : Hakuwa)	
	March 8 (Thu.)	
10:00-11:00	Chairman : Daiji Kimura (National Institute of Technology, Ube College)	
10:00-11:00	Norimi Yokozaki (Tohoku University)	Enhanced axion-photon coupling in GUT with hidden photon
11:00-11:15	Break	
11:15-12:00	Kento Asai (University of Tokyo)	Extension of the Standard Model by a gauged lepton flavor symmetry and leptogenesis
12:00-12:15	Gabriela Barenboim (Valencia,IFIC)	CPT violation and neutrinos

2 Table of contents

- **Dark pion DM : WIMP vs SIMP** p.1–5
  Speaker: Pyungwon Ko (Korea Institute for Advanced Study)
- **Anisotropy of dark matter velocity distribution** p.6–10
  Speaker: Keiko Nagao (National Institute of Technology, Niihama College)
- **Research on Quantum Entanglement of the Vacuum of Fields** p.11–13
  Speaker: Kazushige Ueda (Hiroshima University)
- **Generation of particle number asymmetry in an expanding universe; a novel mechanism** p.14–18
  Speaker: Apriadi Salim Adam (Hiroshima University)
- **Flavor versus mass eigenstates in neutrino asymmetries: implications** p.19–23
  Speaker: Gabriela Barenboim (Valencia, IFIC)
- **Non-Abelian Discrete Groups and Neutrino Flavor Symmetry** p.24–29
  Speaker: Morimitsu Tanimoto (Niigata University)
- **Searches for pseudo Nambu-Goldstone bosons by stimulated resonant photon-photon scatterings with high-intensity laser fields** p.30–34
  Speaker: Kensuke Homma (Hiroshima University)
- **Relation of CLFV to cosmological observables in the CMSSM coannihilation scenario with the seesaw mechanism** p.35–37
  Speaker: Masato Yamanaka (Maskawa Institute Kyoto Sangyo University)
- **Towards the minimal seesaw model for the prediction of neutrino CP violation** p.38–40
  Speaker: Kenta Takagi (Hiroshima University)
- **Enhanced axion-photon coupling in GUT with hidden photon** p.41–45
  Speaker: Norimi Yokozaki (Tohoku University)
- **Extension of the Standard Model by a gauged lepton flavor symmetry and leptogenesis** p.46–48
  Speaker: Kento Asai (University of Tokyo)
- **CPT violation and neutrinos** p.49–51
  Speaker: Gabriela Barenboim (Valencia, IFIC)

Dark pion dark matter : WIMP vs. SIMP

Pyungwon Ko[1]

School of Physics, Korea Institute for Advanced Study,
Seoul 02455, Korea

Abstract

Dark pions from strongly interacting hidden sector can be a good dark matter candidate, either weakly interacting massive particle (WIMP) or strongly interacting massive particle (SIMP), depending on parameters such as dark pion mass and its couplings to the SM fields as well as among themselves. In this talk I discuss both scenarios.

1 Introduction

One of the most pressing questions in particle physics at the moment is to understand dark matter of the universe. So far the existence of DM was confirmed through astrophysical and cosmological observations where only gravitational force plays an important role. Let us first list the relevant questions we have to answer for better understanding of DM from the viewpoint of particle physics described by quantum field theory:

- How many species of DM are there in the universe ?
- What are their masses and spins ?
- Are they absolutely stable or very long-lived ?
- How do they interact among themselves and with the SM particles ?
- Where do their masses come from ?

In order to answer (some of) these questions, we have to observe its signals through nongravitational observations such as colliders and/or various (in)direct detection experiments. There are various ongoing experiments searching for DM particles.

There are many candidates for nonbaryonic dark matter in particle physics: e.g. axion and its supersymmetric partners, sterile neutrinos, gravitino, weakly interacting massive particles (WIMP) [such as the lightest supersymmetric particle (LSP) or the lightest Kaluza-Klein particle (LKP)], and strongly interacting particle (SIMP). And the universe may be filled with cocktails of different species of DM particles.

In this talk, I will concentrate on DM from strongly interacting hidden sector, the so-called hidden (or dark) QCD models (see Fig. 1). In this class of models, flavor and baryon numbers in the hidden sector are accidental symmetries of renormalizable hidden QCD Lagrangian. Then the lightest mesons (let me call it dark pion) and baryons in the hidden sector make DM. Their lifetime could be much longer than the age of the universe because their decays are triggered by dim-5 and dim-6 operators, respectively. Note that dim-5 operators that induce DM decay is dangerous in principle, and we shall assume that its coefficient is small enough to suppress the dark pion decay.

[1]pko@kias.re.kr

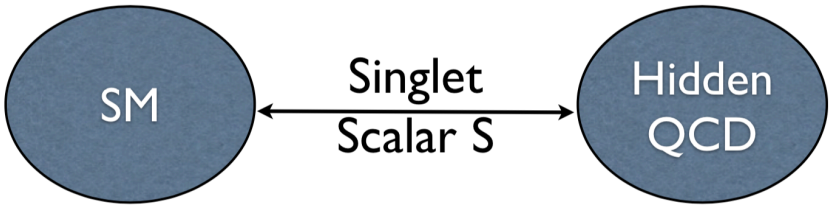

Figure 1: Schematic view of the hidden (dark) QCD model

2 EWSB and CDM from Strongly Interacting Hidden Sector : WIMP scenario

Another nicety of models with strongly interacting hidden sector is that one can construct a model where all the masses of the SM particles and DM are generated by dimensional transmutation in the strongly interacting hidden sector [1, 2, 3, 4]. Basically the light hadron masses such as proton or ρ meson come from confinement, which is derived from massless QCD through dimensional transmutation. One can ask if all the masses of observed particles can be generated by quantum mechanics, in a similar manner with the proton mass in the massless QCD. The most common way to address this question is to employ the Coleman-Weinberg mechanism for radiative symmetry breaking. Here I present a new model based on nonpertubative dynamics like technicolor or chiral symmetry breaking in ordinary QCD (Fig. 1).

Let us consider a scale-invariant extension of the SM with a strongly interacting hidden sector [1, 2, 3, 4]:

$$\begin{aligned}\mathcal{L} &= \mathcal{L}_{\rm SM,kin} + \mathcal{L}_{\rm SM,Yukawa} - \frac{\lambda_H}{4}(H^\dagger H)^2 - \frac{\lambda_{SH}}{2}\, S^2 H^\dagger H - \frac{\lambda_S}{4} S^4 \\ &- \frac{1}{4}\mathcal{G}^a_{\mu\nu}\mathcal{G}^{a\mu\nu} + \sum_{k=1,\ldots,f} \overline{\mathcal{Q}}_k \left[iD\cdot\gamma - \lambda_k S \right] \mathcal{Q}_k. \end{aligned} \quad (1)$$

Here $\mathcal{Q}_k$ and $\mathcal{G}^a_{\mu\nu}$ are the hidden sector quarks and gluons, and and the index k is the flavor index in the hidden sector QCD. We introduced a real singlet scalar S and replaces all the mass parameters by S field in order to respect classical scale symmetry. In this model, we have assumed that the hidden sector strong interaction is vectorlike and confining like the ordinary QCD. Then we can use the known aspects of QCD dynamics to the hidden sector QCD.

In this model, dimensional transmutation will take place in the hidden sector and generate the hidden QCD scale and chiral symmetry breaking with nonzero $\langle \bar{\mathcal{Q}}_k \mathcal{Q}_k \rangle$. Once a nonzero $\langle \bar{\mathcal{Q}}_k \mathcal{Q}_k \rangle$ is developed, the $\lambda_k S$ term generate the linear potential for the real singlet S, which

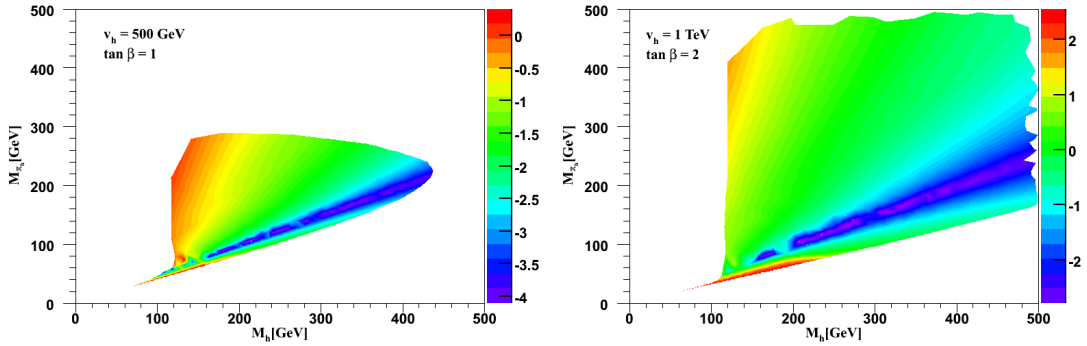

Figure 2: $\Omega_{\pi_h} h^2$ in the (m_{h_1}, m_{π_h}) plane for (a) $v_h = 500$ GeV and $\tan\beta = 1$, and (b) $v_h = 1$ TeV and $\tan\beta = 2$.

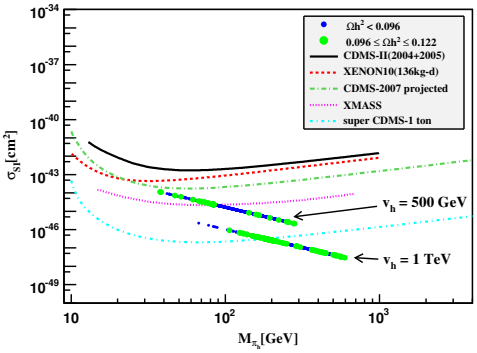

Figure 3: $\sigma_{SI}(\pi_h p \to \pi_h p)$ as functions of m_{π_h}. The upper one is for $v_h = 500$ GeV and $\tan\beta = 1$, and the lower one is for $v_h = 1$ TeV and $\tan\beta = 2$.

in turn results in the nonzero $\langle S \rangle$. Then the hidden sector current quark masses are induced through λ_k terms, and the EWSB can be triggered through λ_{SH} term if it has a correct sign. Then the Nambu-Goldstone boson in the hidden sector, hidden pion or dark pion π_h, will get nonzero masses, and becomes a good CDM candidate. Their dynamics at low energy can be described by chiral Lagrangian method. Also hidden sector baryons $\mathcal{B}_h$ will be formed, the lightest of which would be long lived due to the accidental h-baryon number conservation. Here we consider only the hidden sector pion as dark matter, since dynamics of h-baryons are more difficult to describe in a theoretically systematical way.

Thermail relic denstiy and the spin-independent DM-nucleon scattering cross section relevant for direct detection of DM can be estimated by constructing the chiral Lagrangian for dark pion, including the interactions between dark pions and the SM fields. The results are shown in Figs. 2 and 3, which show that dark pions can be good candidates for WIMP. See Ref. [3, 4] for more details.

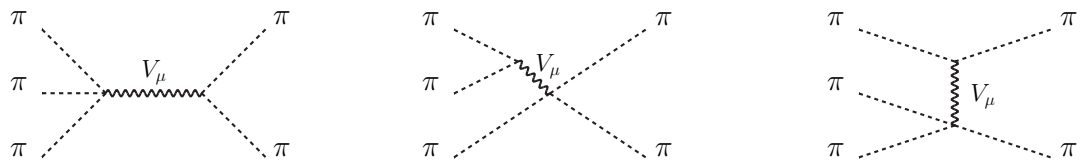

Figure 4: Feynman diagrams contributing to $3 \to 2$ processes for the dark pions with the vector meson interactions.

3 Strongly interacting massive particle (SIMP) scenario within the hidden QCD model

In the original models by Ko *et al.* [1, 2, 3, 4], the Wess-Zumino-Witten (WZW) interaction was not considered. If one includes the WZW term, then the DM number changing processes, $3 \to 2$, becomes possible and one may be able to achieve the correct relic density from this. Also $2 \to 2$ DM self-scattering can be large enough ($\sigma_{\rm self}/m_{\rm DM} \sim O(1)$ barn/GeV) to solve some of the vanilla ΛCDM paradigm, such as the core-cusp puzzle [5]. This new way to achieve both the relic density and the large self scattering cross section is often called Strongly Interacting Massive Particle (SIMP) scenario [6]. However, it turns out that the original proposal by Hochberg et al. for dark pion DM [7] is unlikely to be compatible with the validity of chiral perturbation theory, since one has to have $m_\pi/f_\pi \sim O(4\pi)$.

In Ref. [8], the present author showed that this problem can be significantly relieved if one includes the dark vector mesons (analogy of ρ and ω in the ordinary QCD) because of new $3 \to 2$ diagrams shown in Fig. 4. Also light dark vector mesons make additional contirbutions to the dark pion self scattering through s, t and u-channel exchanges of dark vector mesons. Including these new contributions to the dark pion DM $3 \to 2$ and $2 \to 2$ scatterings from light dark vector mesons and assuming narrow width approximation for them, we find that the phenomenologically viable parameter space is about $m_\pi/f_\pi \sim$ a few (Fig. 5), which is well below 2π, the validity region of the chiral perturbation theory. It is also much smaller than the original proposal $\sim 4\pi f_\pi$ [7].

4 Summary

Summarizing my talk, dark pion DM from strongly interacting hidden sector remains a good DM candidate, whose longevity is due to the accidental flavor symmetry of dark QCD. Depending on the parameter space, one can achieve either WIMP or SIMP scenario.

Acknowledgement The author is grateful to Professor Takuya Morozumi and Professor Yusuke Shimizu for organizing the PPAP2018 in a plesant manner and inviting him with great hospitality. PPAP2018 is sponsored by JSPS Grant-in Aid for Scientific Research (C) Grant Number JP17K05418 and Core of Research for the Energetic Universe (Core-U) of Hiroshima University.

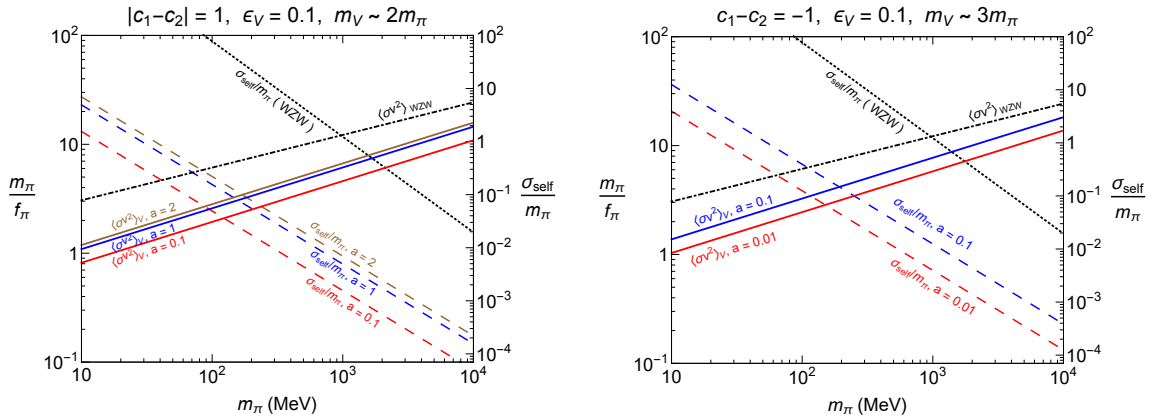

Figure 5: Contours of relic density ($\Omega h^2 \approx 0.119$) for m_π and m_π/f_π and self-scattering cross section per DM mass in cm^2/g as a function of m_π. The case without and with vector mesons are shown in black lines and colored lines respectively. We have imposed the relic density condition for obtaining the contours of self-scattering cross section. Vector meson masses are taken near the resonances with $m_V \approx 2m_\pi$ ($m_V \approx 3m_\pi$) on left (right) plots. In both plots, $c_1 - c_2 = -1$ and $\epsilon_V = 0.1$ are taken. See Ref. [8] for the definitions of these parameters.

References

[1] T. Hur, D. W. Jung, P. Ko and J. Y. Lee, Phys. Lett. B **696**, 262 (2011)

[2] P. Ko, Int. J. Mod. Phys. A **23**, 3348 (2008)

[3] T. Hur and P. Ko, Phys. Rev. Lett. **106**, 141802 (2011)

[4] H. Hatanaka, D. W. Jung and P. Ko, JHEP **1608**, 094 (2016)

[5] S. Tulin and H. B. Yu, Phys. Rept. **730**, 1 (2018)

[6] Y. Hochberg, E. Kuflik, T. Volansky and J. G. Wacker, Phys. Rev. Lett. **113**, 171301 (2014)

[7] Y. Hochberg, E. Kuflik, H. Murayama, T. Volansky and J. G. Wacker, Phys. Rev. Lett. **115**, no. 2, 021301 (2015)

[8] S. M. Choi, H. M. Lee, P. Ko and A. Natale, arXiv:1801.07726 [hep-ph].

Anisotropy of dark matter velocity distribution

Keiko I. Nagao[1] [2]

Okayama University of Science, 1-1 Ridaicho, Kita-ku, Okayama-shi 700-0005 Japan

Abstract

Direct detection of dark matter with directional sensitivity has the potential to discriminate the dark matter velocity distribution. Especially, it will be suitable to discriminate isotropic distribution from anisotropic one. Analyzing data produced with Monte-Carlo simulation, required conditions for the discrimination is estimated. If energy threshold of detector is optimized, $O(10^3-10^4)$ event number is required to discriminate the anisotropy.

1 Introduction

The so-called dark matter accounts for about 27% of the energy density of the Universe. Since it cannot be directly observed, it is supposed to have exceedingly weak interaction with the standard model particles. Weak interacting massive particles (WIMPs) are a promising candidate for dark matter. Several experiments are optimized to direct search for the WIMPs. Directional direct detections of dark matter aims to detect both the recoil energy and direction of the nuclear recoils. The directional detection is expected to improve the background rejection efficiency, and furthermore, to obtain other information of dark matter such as the velocity distribution.

In most of direct searches, the velocity distribution of dark matter is supposed to be isotropic Maxwellian velocity distribution. However, non-Maxwellian distribution had been indicated by some simulations and observations [2-7]. In this study, an anisotropic velocity distribution derived in [4] is adopted;

$$f(v_\phi) = \frac{1-r}{N(v_{0,\mathrm{iso.}})} \exp\left[-v_\phi^2/v_{0,\mathrm{iso.}}^2\right] + \frac{r}{N(v_{0,\mathrm{ani.}})} \exp\left[-(v_\phi-\mu)^2/v_{0,\mathrm{ani.}}^2\right], \tag{1}$$

where v_ϕ is the tangential velocity of dark matter with respect to the galactic rest frame, r is a parameter associated with the anisotropy, $N(v)$ is normalization factor, and $\mu = 150$ km/s. The radial velocity v_r and velocity across the galactic plane v_z are suggested to be the isotropic Maxwellian distribution.

This paper is organized as follows: in Section 2, setup of simulation of dark matter-nucleon scattering in directional detector is described. Results of the numerical simulation are also presented in the section. We conclude in Section 3.

2 Numerical simulation

In Figure 1, a nuclear recoil and associated angles in laboratory frame are shown. The Earth receives dark matter wind, and its direction is taken as z-axis. Scattering angle θ is defined as the angle from z-axis. As a result of Monte-Carlo simulation of dark matter-nucleon scatterings, both the recoil energy E_R and the scattering angle θ are obtained. Thus, in principle, the energy-angular distribution is available. It is also interesting to take a look at angular histogram, which can be obtained in the case that energy resolution of the detector is not so good.

[1] nagao@dap.ous.ac.jp

[2] This report is based on the paper [1].

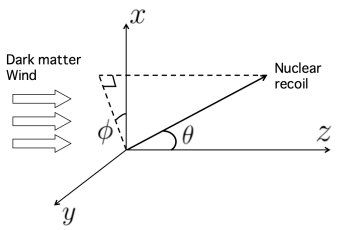

Figure 1: Direction of a nuclear recoil

As a target nucleon, two typical target, fluorine (F) and silver (Ag), are supposed in the simulation. Fluorine is used in gaseous directional detectors, and silver is one of target nucleons in NEWSdm. The strategy is as follows: two kinds of dataset are generated in the Monte-Carlo simulation. One dataset has a large event number, and called as "template data". Template data is produced depending on the anisotropy parameter r, like $r = 0.$ $r = 0.1$, $r = 0.2$, $\cdots$, $r = 1$. The other dataset, which is called as "pseudo-experimental data", is supposed to be data obtained in the realistic experiment, and has smaller event number than template data. Questions are which template is most similar to pseudo-experimental data, and how much event number is required to estimate it. Energy-angular distributions for template data and pseudo-experimental data are produced, and their similarity is tested by chi-squared test in Subsection 2.1. In the chi-squared test, E_R-$\cos\theta$ plane is divided into small bins, and event numbers in each bin. Corresponding chi-squared test for angular histograms is shown in Subsection 2.2. For both the energy-angular distribution and angular histogram, mass relation between WIMP mass m_χ and target nucleon m_N is supposed to be $m_\chi = 3m_N$ for similicity. Also energy threshold of the detector is supposed to be 20 keV for target F, and 50 keV for target Ag.

2.1 Energy-angular distribution

In Figure 2 and 3, results of chi-squared test between template data with particular r and pseudo-experimental data for F and Ag are shown, respectively. Red dashed line represents 90 % confidence level (CL). In the figures, if anisotropic case suggested by N-body simulation $r = 0.3$ is realized, completely isotropic case ($r = 0$) is rejected with 6×10^3 (for F) and 6×10^4 (for Ag) event numbers of the pseudo-experiment. The required event number depends on the energy threshold. Supposed energy thresholds are optimized to reduce the required event numbers of pseudo-experimental data.

2.2 Angular histogram

Angular histogram is another candidate to analyze events in the directional detector. In Figure 4 and 5, chi-squared test of angular histogram for target F and Ag are shown, respectively. Red dashed line corresponds to at the 90% CL. If anisotropic case ($r = 0.3$) is realized, completely isotropic case ($r = 0$) can be rejected at the 90% CL with 5×10^3 (for F) and 2×10^4 (for Ag) event number. Since event number per a bin of energy-angular distribution is smaller than that of angular histogram, required event number is reduced compared to the energy-angular distribution.

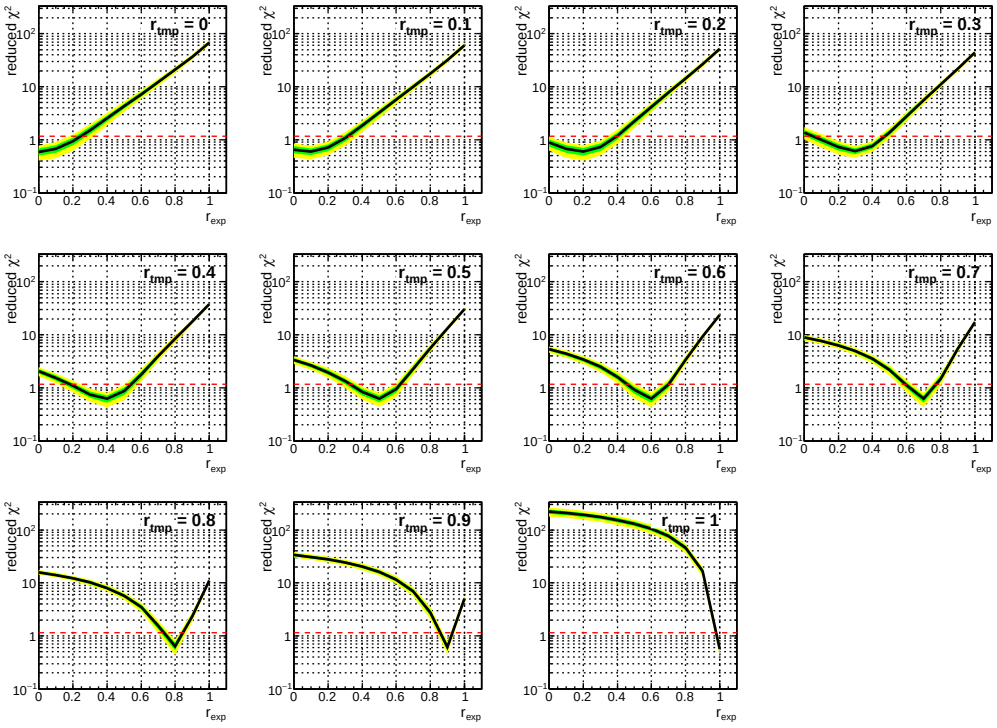

Figure 2: Chi-squared test for target F. The pseudo-experimental data has 6×10^3 event number.

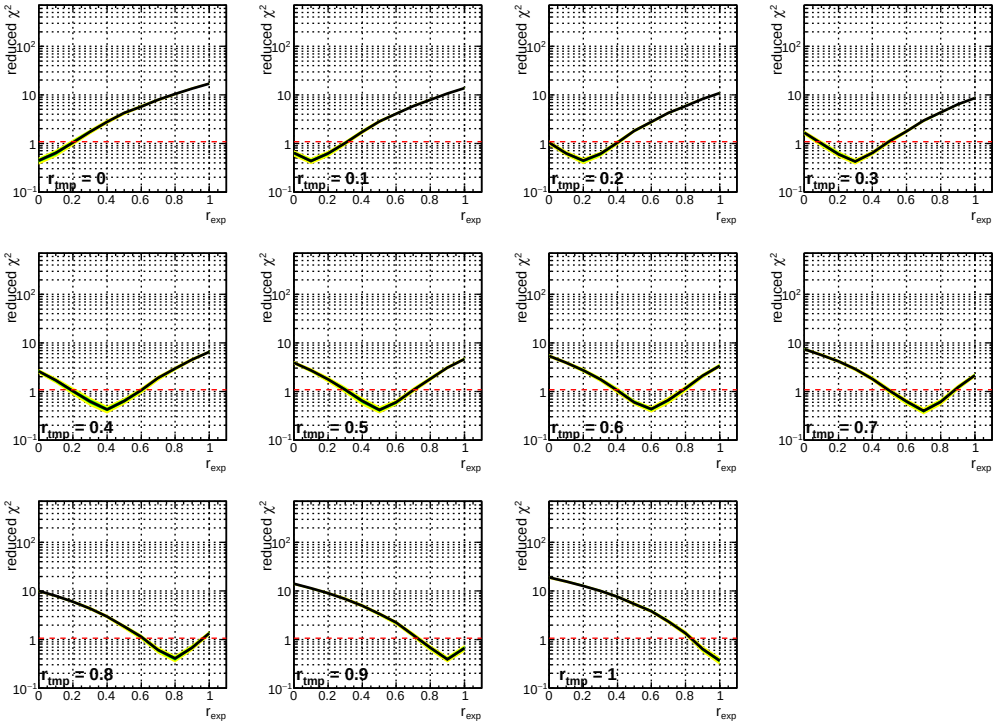

Figure 3: Chi-squared test for target Ag. The pseudo-experimental data has 6×10^4 event number.

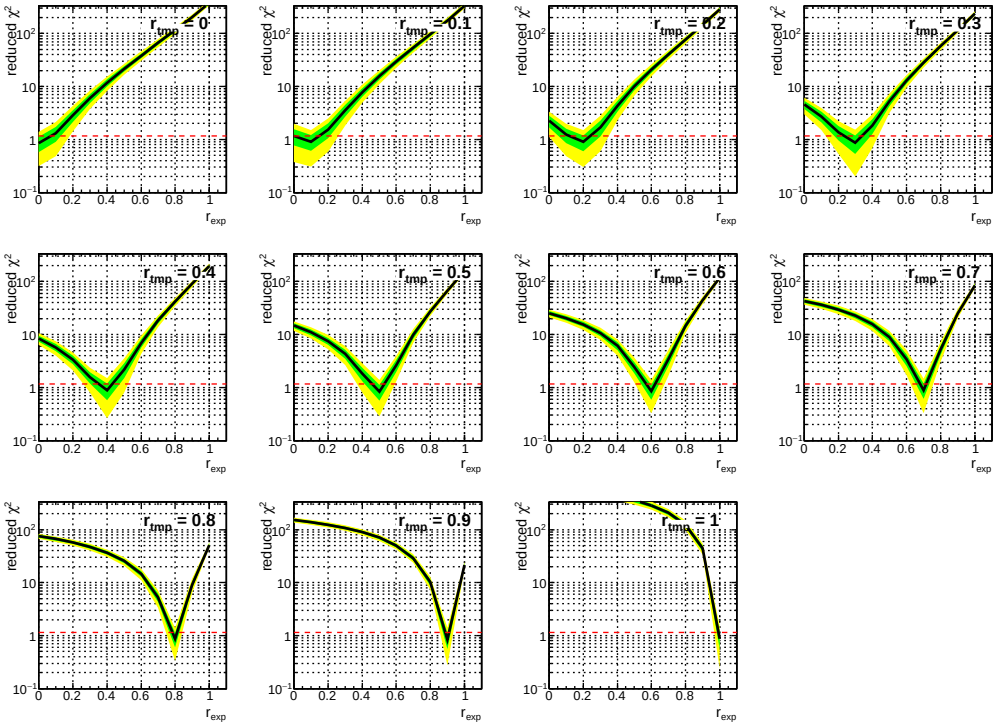

Figure 4: Angular histogram for target F. The pseudo-experimental data has 5×10^3 event number.

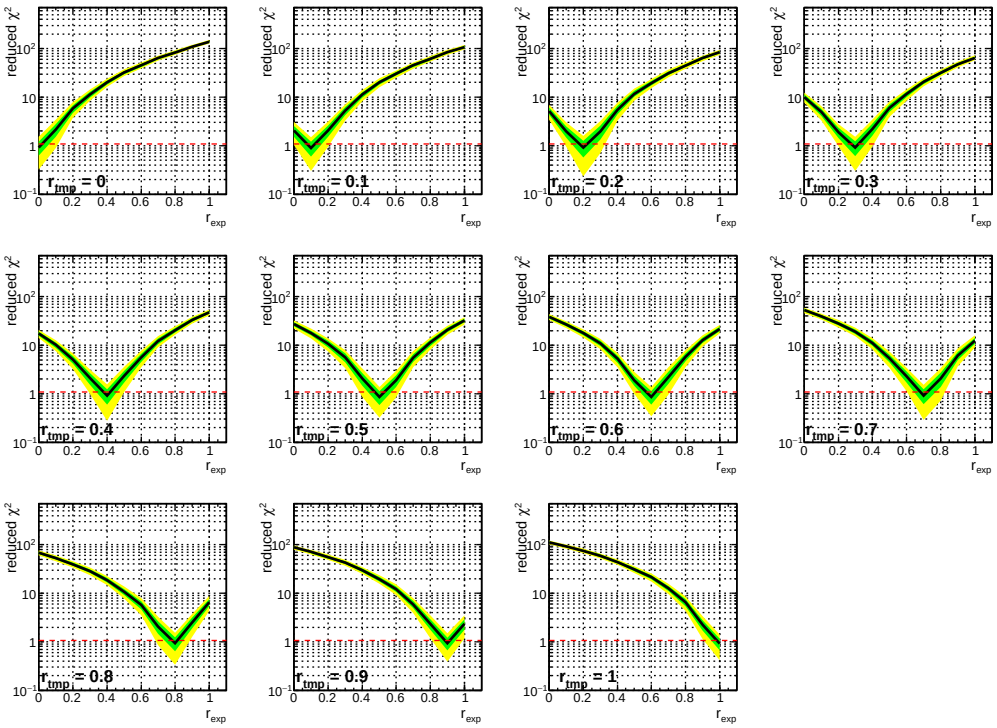

Figure 5: Angular histogmra for target Ag. The pseudo-experimental data has 2×10^4 event number.

3 Conclusion

Possibility to discriminate the anisotropy of dark matter velocity distribution using directional detector is investigated. Depending on resolution of the detector, the energy-angular distribution and angular histogram can be analyzed. For energy-angular distribution case, $O(10^4)$ event number is required, while for angular histogram case $O(10^3 - 10^4)$ is required. It depends on the energy threshold of the detector which is determined by dark matter mass.

References

[1] K. I. Nagao, R. Yakabe, T. Naka and K. Miuchi, arXiv:1707.05523 [hep-ph].

[2] J. I. Read, G. Lake, O. Agertz and V. P. Debattista, Mon. Not. Roy. Astron. Soc. **389**, 1041 (2008) doi:10.1111/j.1365-2966.2008.13643.x.

[3] J. I. Read, L. Mayer, A. M. Brooks, F. Governato and G. Lake, Mon. Not. Roy. Astron. Soc. **397**, 44 (2009) doi:10.1111/j.1365-2966.2009.14757.x.

[4] F. S. Ling, E. Nezri, E. Athanassoula and R. Teyssier, JCAP **1002**, 012 (2010).

[5] M. Maciejewski, M. Vogelsberger, S. D. M. White and V. Springel, Mon. Not. Roy. Astron. Soc. **415**, 2475 (2011) doi:10.1111/j.1365-2966.2011.18871.x.

[6] M. Lisanti and D. N. Spergel, Phys. Dark Univ. **1**, 155 (2012) doi:10.1016/j.dark.2012.10.007.

[7] M. Kuhlen, M. Lisanti and D. N. Spergel, Phys. Rev. D **86**, 063505 (2012) doi:10.1103/PhysRevD.86.063505.

Research on Quantum Entanglement of the Vacuum of Fields

Kazushige Ueda

Graduate School of Science Hiroshima University, 1-3-1 Kagami Yama, Higashi-Hiroshima, Japan 739-8526

Abstract

The quantum entanglement is deeply related to the Unruh effect, which predicts the thermal excitation of the Minkowski vacuum on a curved coordinate. It is well known that the Minkowski vacuum is expressed as an entangled state between the left and right Rindler regions when it is constructed on the Rindler coordinate. We clarify the expression of the Minkowski vacuum extended from the ordinary left and right regions to the entire Minkowski space-time, including the Kasner expanding universe and Kasner shrinking universe. We also investigate the two-dimensional case, and clarify the structure of the quantum entanglement.

1 Introduction

Unruh and Wald pointed that the Minkowski vacuum state is expressed as an entangled state of right Rindler state and left Rindler state[1]. The fact indicates that the entanglement is important to understand the Unruh effect. But the description derived by Unruh and Wald covers only a half of the Minkowski spacetime. Therefore, the description which covers entire Minkowski spacetime is necessary to consider the entanglement of the Minkowski vacuum. This research provide the description.

2 Discussion

We quantize a massless scalar field in each region which is described by Rindler coordinates and Kasner coordinates. The action of massless scalar filed is given by:

$$S = \frac{1}{2}\int d^4x\sqrt{-g}g^{\mu\nu}\partial_\mu\phi\partial_\nu\phi. \tag{1}$$

We used following coordinates to describe entire Minkowski spacetime.

$$\begin{aligned}
&\text{R region}: \ t = \frac{1}{a}e^{a\xi}\sinh a\tau, \ z = \frac{1}{a}e^{a\xi}\cosh a\tau, \ (-\infty < \tau, \xi < \infty) \\
&\text{L region}: \ t = \frac{1}{a}e^{a\tilde{\xi}}\sinh a\tilde{\tau}, \ z = -\frac{1}{a}e^{a\tilde{\xi}}\cosh a\tilde{\tau}, \ (-\infty < \tilde{\tau}, \tilde{\xi} < \infty) \\
&\text{F region}: \ t = \frac{1}{a}e^{a\eta}\cosh a\zeta, \ z = \frac{1}{a}e^{a\eta}\sinh a\zeta, \ (-\infty < \eta, \zeta < \infty) \\
&\text{P region}: \ t = -\frac{1}{a}e^{-a\tilde{\eta}}\cosh a\tilde{\zeta}, \ z = \frac{1}{a}e^{-a\tilde{\eta}}\sinh a\tilde{\zeta}, \ (-\infty < \tilde{\eta}, \tilde{\zeta} < \infty)
\end{aligned}$$

Each coordinates describes a quarter of entire Minkowski spacetime. By constructing the quantized field on each coordinates, we obtain mode functions. We conducted analytic continuation of modes and revealed the relation:

$$v^{\mathrm{I}}_{\omega,\boldsymbol{k}_\perp}(x) = \begin{cases} v^{\mathrm{F,s}}_{\omega,\boldsymbol{k}_\perp} & \mathrm{F} \\ v^{\mathrm{R}}_{\omega,\boldsymbol{k}_\perp} & \mathrm{R} \\ 0 & \mathrm{L} \\ v^{\mathrm{P,d}}_{\omega,\boldsymbol{k}_\perp} & \mathrm{P} \end{cases}, \qquad v^{\mathrm{II}}_{\omega,\boldsymbol{k}_\perp}(x) = \begin{cases} v^{\mathrm{F,d}}_{\omega,\boldsymbol{k}_\perp} & \mathrm{F} \\ 0 & \mathrm{R} \\ v^{\mathrm{L}}_{\omega,\boldsymbol{k}_\perp} & \mathrm{L} \\ v^{\mathrm{P,s}}_{\omega,\boldsymbol{k}_\perp} & \mathrm{P} \end{cases}. \tag{2}$$

Here, the indices F,R,L,P express regions where the mode are. And indices s and d express right moving and left moving. From the relation (2), we can express the mode expansion of scalar field as:

$$\phi(x) = \sum_{\sigma=\mathrm{I,II}} \int_0^\infty d\omega \int_{-\infty}^\infty d^2k_\perp \left(\hat{a}^\sigma_{\omega,\boldsymbol{k}_\perp} v^\sigma_{\omega,\boldsymbol{k}_\perp}(x) + \mathrm{h.c.}\right). \tag{3}$$

Therefore, the description of Minkowski vacuum reduces to

$$|0,\mathrm{M}\rangle = \prod_j \Big[N_j \sum_{n_j=0}^\infty e^{-\pi n_j \omega/a} |n_j,\mathrm{I}\rangle \otimes |n_j,\mathrm{II}\rangle \Big], \tag{4}$$

where $N_j = \sqrt{1-e^{-2\pi\omega/a}}$, and $j = (\omega, \boldsymbol{k}_\perp)$. The form of the Minkowski vacuum is same as the description derived Unruh and Wald. Although, the state of right hand side in eq.(4) is defined in the entire Minkowski spacetime.

We can consider the 2 dimensional case by the almost same procedure. In 2 dimensional case, Minkowski vacuum is consisted of 4 type of mode. The 2 dimensional Minkowski vacuum is expressed as

$$|0,\mathrm{M}\rangle = \prod_\omega \Big[N_\omega \sum_{n_\omega=0}^\infty e^{-\pi n_\omega \omega/a} |n_\omega,\mathrm{I}\rangle \otimes |n_\omega,\mathrm{III}\rangle \Big] \otimes \prod_{\omega'} \Big[N_{\omega'} \sum_{n_{\omega'}=0}^\infty e^{-\pi n_{\omega'} \omega'/a} |n_{\omega'},\mathrm{II}\rangle \otimes |n_{\omega'},\mathrm{IV}\rangle \Big] \tag{5}$$

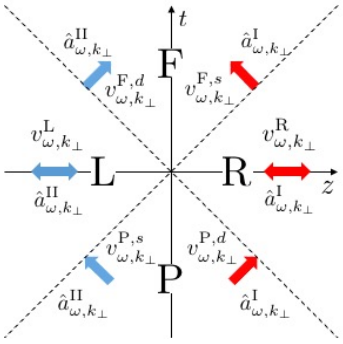

Figure 1: Mode functions (4-D)

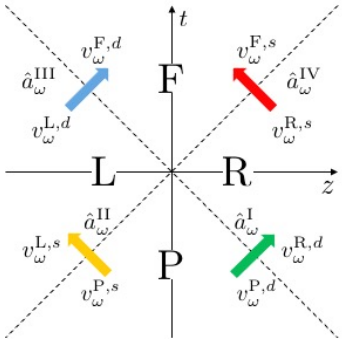

Figure 2: Mode functions (2-D)

The definition of I,II,III,IV in the equation (5) is explained in Figure 2. Figure 1 indicates that the mode of 4 dimensional massless scalar field propagates to timelike direction just like massive wave, which comes from the momentum perpendicular to the direction of acceleration ($\boldsymbol{k}_\perp \neq 0$). On the other hand, the mode of 2 dimensional massless scalar field propagates along with the lightcone. This facts indicates that the wavenumber which corresponds to spacial axis perpendicular to the direction of acceleration plays the role of mass.

Acknowledgement

This talk is based on collaboration with Atsushi Higuchi, Satoshi Iso, Rumi Tatsukawa and Kazuhiro Yamamoto [3, 4]. I express my gratitude to all person who helped me to contribute to this research.

References

[1] W. G. Unruh, R. M. Wald, Phys. Rev. D **29**, 1047 (1984)

[2] L. C. B. Crispino, A. Higuchi, G. E. A. Matsas, Rev. Mod. Phys. **80**, 787 (2008)

[3] S. Iso, R. Tatsukawa, K. Ueda, K. Yamamoto, Phys. Rev. D 96, 045001(2017)

[4] A. Higuchi, S. Iso, K. Ueda, K. Yamamoto, Phys. Rev. D 96, 083531(2017)

Generation of particle number asymmetry in expanding universe[1]

Apriadi Salim Adam[2] and Takuya Morozumi[3]

Graduate School of Science Hiroshima University, 1-3-1 Kagamiyama, Higashi-Hiroshima, 739-8526, Japan
Core of Research for Energetic Universe, Hiroshima University, Higashi-Hiroshima, 739-8526, Japan

Keiko I. Nagao[4]

Okayama University of Science, Faculty of Science, Department of Applied Physics, Okayama, Japan 700-0005

Hiroyuki Takata[5]

Tomsk State Pedagogical University, Tomsk, 634061, Russia

Abstract

We study the creation and time evolution of particle number asymmetry with nonequilibrium quantum field theory. We introduce a model of a neutral scalar and a complex scalar and it has CP violating and particle number violating features. Starting with an initial condition specified by density operator, we show how particle number asymmetry can be generated through interaction. We investigate the time evolution of particle number asymmetry of the universe using the perturbation method.

1 Introduction

What still not yet fully understood from the standard model (SM) point of view is why there is more baryon than anti-baryon in the universe [1]. In order to address this issue, a number of studies have been proposed [2]. In present work, we study a model which generates particle number asymmetry through interactions and develop a formulation which is applicable to various types of expanding universe [3, 4]. In addition, we also compute the time evolution of current asymmetry by using quantum field theory with the density operator.

2 The model

The model consists of a neutral scalar, N, and a complex scalar, ϕ. The action S is given by [3, 4],

$$\begin{aligned} S =& \int d^4x\sqrt{-g}\left(\mathcal{L}_{\rm free}+\mathcal{L}_{\rm int}+\xi(R-2\Lambda)\right), \\ \mathcal{L}_{\rm free} =& g^{\mu\nu}\nabla_\mu\phi^\dagger\nabla_\nu\phi - m_\phi^2|\phi|^2+\frac{1}{2}\nabla_\mu N\nabla^\mu N-\frac{M_N^2}{2}N^2+\frac{B^2}{2}(\phi^2+\phi^{\dagger 2}) \\ &+\left(\frac{\alpha_2}{2}\phi^2+h.c.\right)R+\alpha_3|\phi|^2R, \\ \mathcal{L}_{\rm int} =& A\phi^2N+A^*\phi^{\dagger 2}N+A_0|\phi|^2N, \end{aligned} \tag{1}$$

[1] contributed talk at 1st workshop on Phenomenology for Particle and Anti-Particle 2018 (PPAP 2018)

[2] apriadiadam@hiroshima-u.ac.jp
[3] morozumi@hiroshima-u.ac.jp
[4] nagao@dap.ous.ac.jp
[5] takata@tspu.edu.ru

where A is the interaction coupling of the vertex, B is the parameter which gives the mass difference of the fields and α_2 is the matter-curvature coupling. The metric $g_{\mu\nu}$ is given by the type of Friedmann Robertson Walker with scale factor $a(x^0)$,

$$g_{\mu\nu} = (1, -a^2(x^0), -a^2(x^0), -a^2(x^0)), \tag{2}$$

while R is the Riemann curvature which has form $R = 6\left[\left(\frac{\ddot{a}}{a}\right) + \left(\frac{\dot{a}}{a}\right)^2\right]$ and $H(x^0) = \frac{\dot{a}}{a}$. With the Lagrangian in Eq.(1), we study the particle number asymmetry produced by the soft-breaking terms of U(1) symmetry whose coefficients are denoted by A and B^2. Noticing that, with this Lagrangian, one can also derive the Einstein equations for the scale factor coupled with scalar particles. They are given as,

$$T_{\mu\nu} = \partial_\mu\phi_i\partial_\nu\phi_i - g_{\mu\nu}\left(\frac{1}{2}g^{\alpha\beta}\partial_\alpha\phi_i\partial_\beta\phi_i - \frac{1}{2}m_i^2\phi_i^2 + \frac{1}{3}A_{ijk}\phi_i\phi_j\phi_k\right) \tag{3}$$

$$-3(1 - 8\pi G\beta_i\phi_i^2)\left(\frac{\dot{a}}{a}\right)^2 + \Lambda = -8\pi G T_{00} \text{ (00 component)} \tag{4}$$

$$(1 - 8\pi G\beta_i\phi_i^2)(2a\ddot{a} + \dot{a}^2) - a^2\Lambda = -8\pi G T_{ii} \text{ (ii component)} \tag{5}$$

$$0 = -8\pi G T_{\mu\nu(\neq\mu)} \text{ (off diagonal component)} \tag{6}$$

However, a full discussion for solving them lies beyond the scope of this study. At present, we work for the case that the time dependence of the scale factor is given.

3 The current expectation value and its time evolution

The particle number is related to U(1) transformation of the complex scalar field, namely, $\phi(x) \to \phi(x)e^{i\theta}$. It is U(1) charge represented by particle number operator N [5],

$$N(x^0) = \int \sqrt{-g(x)}j_0(x)d^3\mathbf{x} \tag{7}$$

$$j_\mu(x) = i(\phi^\dagger\partial_\mu\phi - \partial_\mu\phi^\dagger\phi). \tag{8}$$

As for the initial condition of the state, it is given by density operator, namely,

$$\rho(t_0) = \frac{e^{-H_0/T}}{\mathrm{tr}e^{-H_0/T}}, \tag{9}$$

where H_0 is a Hamiltonian includes the linear term of the fields and T denotes the temperature.

It is convenient to write the scalar particles in terms of real fields by using the following relations, $\phi \equiv \frac{\phi_1 + i\phi_2}{\sqrt{2}}$ and $\phi_3 \equiv N$. In terms of real fields, the current expectation value written with initial density operator has form,

$$\begin{aligned}\langle j_\mu(x)\rangle &= \mathrm{tr}(j_\mu(x)\rho(t_0)),\\ &= \mathrm{Re.}\left[\left(\frac{\partial}{\partial x^\mu} - \frac{\partial}{\partial y^\mu}\right)G_{12}(x,y)\Big|_{y\to x} + \bar{\phi}_2^*(x)\overset{\leftrightarrow}{\partial_\mu}\bar{\phi}_1(x)\right],\end{aligned} \tag{10}$$

where $\bar{\phi}$ denotes the mean field with a relation, $\phi = \bar{\phi} + \varphi$. Both Green's function and field are obtained from 2PI effective action Γ_2 [6],

$$\Gamma_2[G, \bar{\phi}, g] = S[\bar{\phi}, g] + \frac{i}{2}\mathrm{TrLn}\ G^{-1} + \Gamma_Q - \frac{i}{2}\mathrm{Tr}\ \mathbf{1} + \frac{1}{2}\int d^4x\int d^4y\frac{\delta^2 S[\bar{\phi}, g]}{\delta\bar{\phi}_i^a(x)\delta\bar{\phi}_j^b(y)}G_{ij}^{ab}(x,y), \tag{11}$$

where Γ_Q is the lowest order of 2PI diagram. Their equations of motion are derived by taking derivative Γ_2 with respect to Green's function and field, respectively.

Before closing this section, let us write down the time evolution of the current asymmetry. First, we consider the solution of Green's function and field up to the first order of interaction coupling A and up to the linear order of the Hubble constant $H(t_0)$. In this case, we focus on the case that the initial expectation value of the field is $(\bar{\phi}_1, \bar{\phi}_2, \bar{\phi}_3) = (0, 0, v_3)$. Then, the contribution to the current asymmetry is only given by the first term of Eq.(10),

$$\begin{aligned}\langle j_0(x^0)\rangle_{O(A)} =& \int \frac{d^3k}{(2\pi)^3}\left(\frac{\partial}{\partial x^0} - \frac{\partial}{\partial y^0}\right)[\mathrm{Re}.\hat{G}_{12}^{O(A)}(x^0, y^0, \mathbf{k})]\big|_{y^0\to x^0}, \\ =& \langle j_0(x^0)\rangle_{1\mathrm{st}} + \langle j_0(x^0)\rangle_{2\mathrm{nd}},\end{aligned} \tag{12}$$

where $\langle j_0(x^0)\rangle_{1\mathrm{st}}$ and $\langle j_0(x^0)\rangle_{2\mathrm{nd}}$ are given by,

$$\begin{aligned}\langle j_0(x^0)\rangle_{1\mathrm{st}} =& \frac{2v_3 A_{123}}{a_{t_0}^3}\int\frac{d^3\mathbf{k}}{(2\pi)^3}\int_{t_0}^{x^0}\left\{1 - 3(x^0 - t_0)H(t_0) - \frac{3}{2}(t - t_0)H(t_0)\right\} \\ &\times\left[\left\{\frac{(-\bar{K}^{(0)\prime}_{3,tt_0,\mathbf{0}})}{2\omega_{2,\mathbf{k}}(t_0)}\coth\frac{\beta\omega_{2,\mathbf{k}}(t_0)}{2}\left[\left(\bar{K}^{(0)\prime}_{2,x^0t_0,\mathbf{k}}\overset{\leftrightarrow}{\partial}\cdot\bar{K}^{(0)}_{1,x^0t,\mathbf{k}}\right)\bar{K}^{(0)\prime}_{2,tt_0,\mathbf{k}}\right.\right. \\ &\left.\left.+\omega_{2,\mathbf{k}}^2(t_0)\left(\bar{K}^{(0)}_{2,x^0t_0,\mathbf{k}}\overset{\leftrightarrow}{\partial}\cdot\bar{K}^{(0)}_{1,x^0t,\mathbf{k}}\right)\bar{K}^{(0)}_{2,tt_0,\mathbf{k}}\right]\right\} - \{1\leftrightarrow 2 \text{ for lower indices}\}\Bigg]\,dt,\end{aligned} \tag{13}$$

$$\begin{aligned}\langle j_0(x^0)\rangle_{2\mathrm{nd}} =& \frac{2v_3 A_{123}}{a_{t_0}^3}\int\frac{d^3\mathbf{k}}{(2\pi)^3}\int_{t_0}^{x^0}\left[\left\{\frac{(-\bar{K}^{(0)\prime}_{3,tt_0,\mathbf{0}})}{2\omega_{2,\mathbf{k}}(t_0)}\coth\frac{\beta\omega_{2,\mathbf{k}}(t_0)}{2}\right.\right. \\ &\times\left[\left(\bar{K}^{(0)\prime}_{2,x^0t_0,\mathbf{k}}\overset{\leftrightarrow}{\partial}\cdot\bar{K}^{(0)}_{1,x^0t,\mathbf{k}}\right)\bar{K}^{(1)\prime}_{2,tt_0,\mathbf{k}} + \left(\bar{K}^{(1)\prime}_{2,x^0t_0,\mathbf{k}}\overset{\leftrightarrow}{\partial}\cdot\bar{K}^{(0)}_{1,x^0t,\mathbf{k}} + \bar{K}^{(0)\prime}_{2,x^0t_0,\mathbf{k}}\overset{\leftrightarrow}{\partial}\cdot\bar{K}^{(1)}_{1,x^0t,\mathbf{k}}\right)\bar{K}^{(0)\prime}_{2,tt_0,\mathbf{k}}\right. \\ &+\omega_{2,\mathbf{k}}^2(t_0)\left[\left(\bar{K}^{(0)}_{2,x^0t_0,\mathbf{k}}\overset{\leftrightarrow}{\partial}\cdot\bar{K}^{(0)}_{1,x^0t,\mathbf{k}}\right)\bar{K}^{(1)}_{2,tt_0,\mathbf{k}}\right. \\ &\left.\left.\left.\left.+\left(\bar{K}^{(1)}_{2,x^0t_0,\mathbf{k}}\overset{\leftrightarrow}{\partial}\cdot\bar{K}^{(0)}_{1,x^0t,\mathbf{k}} + \bar{K}^{(0)}_{2,x^0t_0,\mathbf{k}}\overset{\leftrightarrow}{\partial}\cdot\bar{K}^{(1)}_{1,x^0t,\mathbf{k}}\right)\bar{K}^{(0)}_{2,tt_0,\mathbf{k}}\right]\right]\right\} - \{1\leftrightarrow 2 \text{ for lower indices}\}\Bigg]\,dt.\end{aligned} \tag{14}$$

where $\bar{K}_i[x^0, y^0]$ and its derivative are given by,

$$\bar{K}_i^{(0)}[x^0, y^0] = \frac{\sin[\omega_{i,\mathbf{k}}(x^0 - y^0)]}{\omega_{i,\mathbf{k}}}, \quad \omega_{i,\mathbf{k}} = \sqrt{\frac{\mathbf{k}^2}{a(t_0)^2} + \tilde{m}_i^2},$$

$$\tilde{m}_1^2 = m_\phi^2 - B^2, \quad \tilde{m}_2^2 = m_\phi^2 + B^2, \quad \tilde{m}_3^2 = m_N^2, \tag{15}$$

$$\bar{K}_i^{(1)}[x^0, y^0] = \frac{H(t_0)\mathbf{k}^2(x^0 + y^0 - 2t_0)}{2\omega_{i,\mathbf{k}}^2 a(t_0)^2}\left(\frac{\sin[\omega_{i,\mathbf{k}}(x^0 - y^0)]}{\omega_{i,\mathbf{k}}} - (x^0 - y^0)\cos[\omega_{i,\mathbf{k}}(x^0 - y^0)]\right), \tag{16}$$

$$\bar{K}_i'[x^0, y^0] := \frac{\partial\bar{K}_i[x^0, y^0]}{\partial y^0}, \quad \dot{\bar{K}}_i[x^0, y^0] := \frac{\partial\bar{K}_i[x^0, y^0]}{\partial x^0}, \quad \dot{\bar{K}}_i'[x^0, y^0] := \frac{\partial^2\bar{K}_i[x^0, y^0]}{\partial x^0\partial y^0}, \tag{17}$$

From Eqs.(13) and (14), below we remark several findings:

1. In the first line of Eq.(13), the first, second and third terms in wave parentheses correspond to the contribution of constant scale factor to the current asymmetry, dilution effect and freezing interaction effect, respectively.

2. Eq.(14) corresponds to the redshift effect for the contribution to the current asymmetry.

Table 1: The classification of $o(H(t_0))$ contributions to the current asymmetry

The effect	The origin
Dilution	The increase of volume of the universe due to expansion, $\frac{1}{a(x^0)^3} - \frac{1}{a(t_0)^3}$
Freezing interaction	The decrease of the strength of the cubic interaction as $\left\{ \left(\frac{a(t_0)}{a(x^0)} \right)^{3/2} - 1 \right\} A_{123}$.
Redshift	The effective energy of particle, $\frac{\mathbf{k}^2}{a(x^0)^2} + \tilde{m}_i^2$.

The above four types of the contribution to the current asymmetry are explained as follows. The constant scale factor which is the zeroth order of $H(t_0)$ is the leading contribution. The rests which are the first order term contribute according to their origins and we summarize them in Table 1. In the next section, we study numerically the time evolution of the current asymmetry.

4 Numerical results

In the left side of Fig.1, we show the parameter B dependence. Both of the amplitude and the period of the oscillation change when we alter the parameter B. As it increases, the amplitude becomes larger and its period becomes shorter. The right side of Fig.1 shows the dependence of the PNA on $\omega_{3,\mathbf{0}}$. As shown in the black, blue and dot-dashed blue lines, the position of the first node does not change when $\omega_{3,\mathbf{0}}$ takes its value within the difference of $\tilde{m}_1$ and $\tilde{m}_2$. However, the amplitude of oscillation gradually decreases as $\omega_{3,\mathbf{0}}$ increases up to the mass difference. The interesting findings were observed when $\omega_{3,\mathbf{0}}$ becomes larger than the mass difference. As $\omega_{3,\mathbf{0}}$ becomes larger, the amplitude decreases and the new node is formed at once. The dashed and dotted blue lines show this behavior.

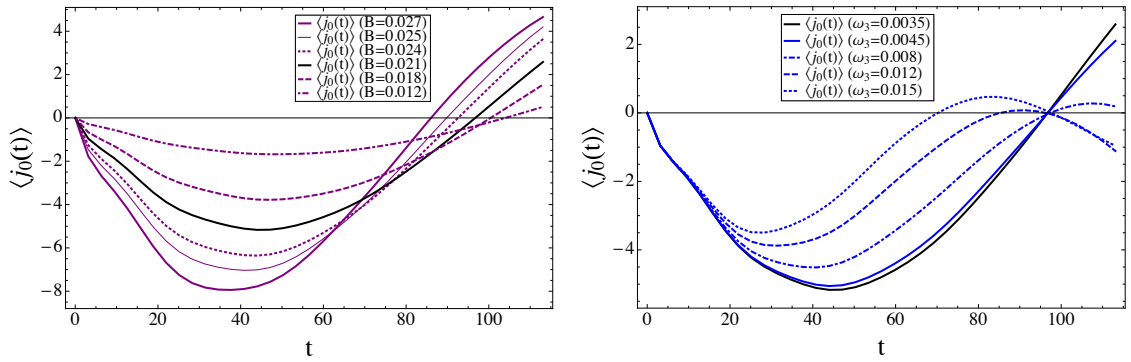

Figure 1: B dependence (left) and $\omega_{3,\mathbf{0}}$ dependence (right) for the time evolution of PNA are displayed. In both figures, the horizontal axis is the dimensionless time defined as $t = \omega^r_{3,\mathbf{0}}(x^0 - t_0)$ and we choose $\omega^r_{3,\mathbf{0}} = 0.35$ as a reference angular frequency. In the left figure, we fix a set of parameters as $(\tilde{m}_2, T, H_{t_0}, \omega_{3,\mathbf{0}})$=$(0.05, 100, 10^{-3}, 0.0035)$ for all the lines. In the right figure, we use a set of parameters as $(\tilde{m}_1, \tilde{m}_2, B, T, H_{t_0})$=$(0.04, 0.05, 0.021, 100, 10^{-3})$ for all the lines [4].

5 Conclusion

We have studied an interacting model in which particle number asymmetry is generated through interactions of scalar fields. The current for the particle and anti-particle asymmetry is given up to the first order of A and linear $H(t_0)$. Time evolution of the particle number asymmetry and its parameter dependence is investigated.

Acknowledgement This work is supported by JSPS KAKENHI Grant Number JP17K05418 (T.M.) and supported in part by JSPS Grant-in-Aid for Scientific Research for Young Scientists (B) 26800151 (K.I.N.).

References

[1] J. P. Kneller and G. Steigman, New Journal of Physics **6**, 117 (2004); P. A. R. Ade and others, Astron. Astrophys. **594**, A13 (2016).

[2] M. Yoshimura, Phys. Rev. Lett. **41**, 281 (1978); M. Fukugita and T. Yanagida, Phys. Lett. B **174**, 45 (1986); D. Zhuridov, Phys. Rev. D **94**, 035007 (2016); N. Blinov and A. Hook, Phys. Rev. D **95**, 095014 (2017).

[3] T. Morozumi, K. I. Nagao, A. S. Adam and H. Takata, Russ. Phys. J **59**, 1852 (2017), arXiv:1609.02990 [hep-ph].

[4] T. Morozumi, K. I. Nagao, A. S. Adam and H. Takata, arXiv:1709.08781 [hep-th], to be published in Advances in High Energy Physics.

[5] I. Affleck and M. Dine, Nucl. Phys. B **249**, 361 (1985).

[6] S. A. Ramsey and B. L. Hu, Phys. Rev. D **56**, 661 (1997); E. A. Calzetta and B. L. Hu, Nonequilibrium Quantum Field Theory (Cambridge Univ. Press, 2008).

Flavor versus mass eigenstates in neutrino asymmetries (a question of coherence)

Gabriela Barenboim*
Departament de Física Teòrica and IFIC, Universitat de València-CSIC, E-46100, Burjassot, Spain

We show that, if they exist, lepton number asymmetries (L_α) of neutrino flavors should be distinguished from the ones (L_i) of mass eigenstates as cosmological (BBN) bounds on the latters (formers) cannot be directly applied to the formers (latters). Due to the difference of mass and flavor eigenstates, the cosmological constraint on the asymmetries of neutrino flavors can be much stronger than conventional expectation.

INTRODUCTION

A large lepton number asymmetry of neutrinos is an intriguing possibility in regard of its capability of resolving several non-trivial issues of cosmology (see for example [1–3]), but has been known to be constrained tightly by BigBang nucleosynthesis (BBN) [4, 5]. However[6–8], even if BBN constrains the lepton number asymmetry of electron-neutrino very tightly such as $L_e \lesssim \mathcal{O}(10^{-3})$, much larger muon- and tau-neutrino asymmetries of $\mathcal{O}(0.1-1)$ are still allowed as long as the total lepton number asymmetry is sizable. Such large asymmetries are expected to be constrained mainly by cosmic microwave background (CMB) via the extra neutrino species $\Delta N_{\rm eff}$ [9].

If asymmetric neutrinos have a thermal distribution, their contributions to $\Delta N_{\rm eff}$ is expressed as

$$\Delta N_{\rm eff} = \frac{15}{7}\sum_\alpha \left(\frac{\xi_\alpha}{\pi}\right)^2 \left[2+\left(\frac{\xi_\alpha}{\pi}\right)^2\right] \qquad (1)$$

where $\xi_\alpha \equiv \mu_\alpha/T$ is the neutrino degeneracy parameter. Conventionally, the summation in Eq. (1) has been done with neutrino flavors ($\nu_{e,\mu,\tau}$ in case of only three active neutrinos). An implicit assumption here is that the extra radiation energy coming from asymmetric neutrinos are solely from flavor-eigenstates. However, due to neutrino flavor oscillations, the equilibrium density matrix is not diagonal in the flavour basis (as one naively expects, not being the flavour eigestates the asymptotic states of the Hamiltonian) and their description in terms of only diagonal components (a more or less hidden asspumtion when assuming thermal distribution for flavors) cannot capture all the contributions to the extra radiation energy density. On the other hand, well after their decoupling from thermal bath, free-streaming neutrinos should be described as incoherent mass-eigenstates only. Hence, the appropriate estimation of $\Delta N_{\rm eff}$ could be done exclusively with neutrino's mass-eigenstates instead of flavor-eigenstates in Eq. (1).

Let's see why. A standard neutrino flavour transition, or "oscillation", can be understood as follows. A neutrino is produced by a source together with a charged lepton $\overline{\ell_\alpha}$ of flavour α. Therefore, at the production point, the neutrino is a ν_α. Then, after birth, the neutrino travels a distance L until it is detected. There, it is where it reaches a target with which it interacts and produces another charged lepton ℓ_β of flavour β. Thus, at the interaction point, the neutrino is a ν_β. If $\beta \neq \alpha$ (for example, if ℓ_α is a μ but ℓ_β is a τ), then, during its trip from the source to the detection point, the neutrino has transitioned from a ν_α into a ν_β.

This morphing of neutrino flavour, $\nu_\alpha \longrightarrow \nu_\beta$, is a text-book example of a quantum-mechanical effect.

Because, a ν_α is really a coherent superposition of mass eigenstates ν_i,

$$|\nu_\alpha> = \sum_i U^*_{\alpha i}\,|\nu_i> \quad . \qquad (2)$$

the neutrino that propagates since it is created until it interacts, can be any one of the ν_i's, therefore we must add the contributions of all the different ν_i coherently. Then, the transition amplitude, $\mathrm{Amp}(\nu_\alpha \longrightarrow \nu_\beta)$ contains a share of each ν_i and it is a product of three factors. The first one is the amplitude for the neutrino born at the production point in combination with an $\overline{\ell_\alpha}$ to be, specifically, a ν_i. This amplitude is given by $U^*_{\alpha i}$. The second factor is the amplitude for the ν_i created by the source to propagate until it reaches the detector. We will call this factor $\mathrm{Prop}(\nu_i)$. It is not difficult to see that

$$\mathrm{Prop}(\nu_i) = \exp[-i m_i^2 \frac{L}{2E}] \quad . \qquad (3)$$

The third factor is the amplitude for the charged lepton produced by the interaction of the ν_i with the detector to be, specifically, an ℓ_β, which is $U_{\beta i}$. Therefore the amplitude for a neutrino born as a ν_α to be detected as a ν_β after covering a distance L through vacuum with energy E yields

$$\mathrm{Amp}(\nu_\alpha \longrightarrow \nu_\beta) = \sum_i U^*_{\alpha i}\, e^{-i m_i^2 \frac{L}{2E}} U_{\beta i} \quad . \qquad (4)$$

The expression above is valid for an arbitrary number of neutrino flavours and mass eigenstates. The probability $\mathrm{P}(\nu_\alpha \longrightarrow \nu_\beta)$ for $\nu_\alpha \longrightarrow \nu_\beta$ can be found by squaring it,

giving

$$\begin{aligned}
&\mathrm{P}(\nu_\alpha \longrightarrow \nu_\beta) = |\mathrm{Amp}(\nu_\alpha \longrightarrow \nu_\beta)|^2 \\
&= \delta_{\alpha\beta} - 4\sum_{i>j} \Re(U^*_{\alpha i} U_{\beta i} U_{\alpha j} U^*_{\beta j}) \sin^2\left(\Delta m^2_{ij} \frac{L}{4E}\right) \\
&\quad + 2\sum_{i>j} \Im(U^*_{\alpha i} U_{\beta i} U_{\alpha j} U^*_{\beta j}) \sin\left(\Delta m^2_{ij} \frac{L}{2E}\right) \quad , (5)
\end{aligned}$$

with

$$\Delta m^2_{ij} \equiv m^2_i - m^2_j \quad . \tag{6}$$

In order to get Eq. (5) we have used that the mixing matrix U is unitary.

So far, we have been working in natural units, if we return now the $\hbar$'s and c factor (we have happily left out) into the oscillation probability we find that

$$\sin^2\left(\Delta m^2_{ij} \frac{L}{4E}\right) \quad \longrightarrow \quad \sin^2\left(\Delta m^2_{ij} c^4 \frac{L}{4\hbar c E}\right) \tag{7}$$

Having done that, it is easy and instructive to explore the semi-classical limit, $\hbar \longrightarrow 0$. In this limit the oscillation length goes to zero (the oscillation phase goes to infinity) and the oscillations are averaged out. Neutrino propagate as effectively incoherent mass eigenstates. The interference pattern is lost. We no longer talk about oscillations but about flavour transitions. The same happens if we let the mass difference Δm^2 become large or when the distance traveled or the time ellapsed is huge, as it is the case with the cosmic neutrino background after neutrino decoupling.

LEPTON NUMBER ASYMMETRIES OF NEUTRINO FLAVOR VS. MASS EIGENSTATES

The lepton number asymmetries of neutrinos in flavor basis can be defined as a matrix such as

$$\mathbf{L}_\mathrm{f} = \frac{\rho - \bar{\rho}}{n_\gamma} \tag{8}$$

where $\rho/\bar{\rho}$ and n_γ are the density matrices of neutrinos/anti-neutrinos and the photon number density. In the very early universe, it is natural to assume that neutrinos are in interaction eigenstates (i.e., flavor eigenstates), since their kinematic phases are very small and collisional interactions to thermal bath are large enough to block flavor oscillations. Hence, if it were generated by certain mechanism at very high energy, $\mathbf{L}_\mathrm{f}$ is likely to be diagonal and to remain constant. After all while oscillations are blocked, individual flavor lepton numbers are conserved. However, due to the fact that neutrino are not massless and mix, according to the values of the mixing parameters and mass differences measured by a variety of experiments [10] , as the temperature of the radiation dominated universe drops below around $T \sim 15\,\mathrm{MeV}$, flavor oscillations becomes active. $\mathbf{L}_\mathrm{f}$ starts evolving at this epoch, and settles down to an equilibrium state finally at $T \sim 2\,\mathrm{MeV}$ before BBN starts [4, 11–15].

Once it reaches its final equilibrium value, $\mathbf{L}_\mathrm{f}$ becomes time-independent. The shape of $\mathbf{L}_\mathrm{f}$ at the final equilibrium is determined by various effects including vacuum oscillation, MSW-like effect coming from charged lepton backgrounds, neutrinos self-interaction and collisional scattering. So, it is difficult to be predicted analytically, and in practice, only accesible via numerical methods. However, all these effects except vacuum oscillations are active during particular windows in temperature and eventually disappear. Hence, the final shape of $\mathbf{L}_\mathrm{f}$ should be determined by vacuum oscillation parameters only. Note that the flavor states mixed by vacuum oscillation parameters are nothing but mass-eigenstates in flavor-basis. Therefore, the statistical equilibrium state of $\mathbf{L}_\mathrm{f}$ should be that of mass-eigenstates expressed in the flavor-basis.

Since in vacuum mass- and flavor-eigenstates are related to each other by PMNS matrix, U_PMNS [16, 17], our argument implies that for a diagonalization matrix D, $\mathbf{L}_\mathrm{m}$ the matrix of asymmetries in mass basis is given by

$$\mathbf{L}_\mathrm{m} = D\mathbf{L}_\mathrm{f}D^{-1} = U^{-1}_\mathrm{PMNS}\mathbf{L}_\mathrm{f}U_\mathrm{PMNS} \tag{9}$$

implying $D = U^{-1}_\mathrm{PMNS}$.

On general grounds, at late times we do not expect $\mathbf{L}_\mathrm{f}$ to be diagonal. The operator responsible for the evolution of the density matrix is not diagonal, so that a diagonal density matrix will not be the asymptotic solution of those equations unless it is proportional to the identity matrix, which is clearly not the case. Hence, generically the asymmetries of neutrino mass eigenstates differ from those of flavor, and this fact should be taken into account when observational constraints on lepton number asymmetries are considered.

In order to verify our argument, we solved numerically the quantum kinetic equations of neutrino/anti-neutrino density matrices in a simplified way as done in Ref. [6]. An example is shown in Fig. 1 where one finds the evolutions of $L_{\alpha\beta}$, the entries of $\mathbf{Re}\,[\mathbf{L}_\mathrm{f}]$. The change across e^+e^--annihilation around $T \sim 2\,\mathrm{MeV}$ (or $x \sim 0.5$) was taken into account as a global suppression factor $4/11$ for simplicity. As shown in the right panel of the figure, the off-diagonal entries of $\mathbf{Re}\,[\mathbf{L}_\mathrm{f}]$ do not disappear, making $\mathbf{L}_\mathrm{m}$ be different from $\mathbf{L}_\mathrm{f}$. Also, we found that the numerical simulation reproduces the relation $D = U^{-1}_\mathrm{PMNS}$ quite precisely within errors of $\mathcal{O}(0.1)\%$ even at $x = 1$.

The differences between diagonal entries of $\mathbf{L}_\mathrm{f}$ and $\mathbf{L}_\mathrm{m}$ can be seen by expressing the former in terms of the latter. At first, L_e is given by

$$L_e = c^2_{13}\left(c^2_{12}L_1 + s^2_{12}L_2\right) + s^2_{13}L_3 \tag{10}$$

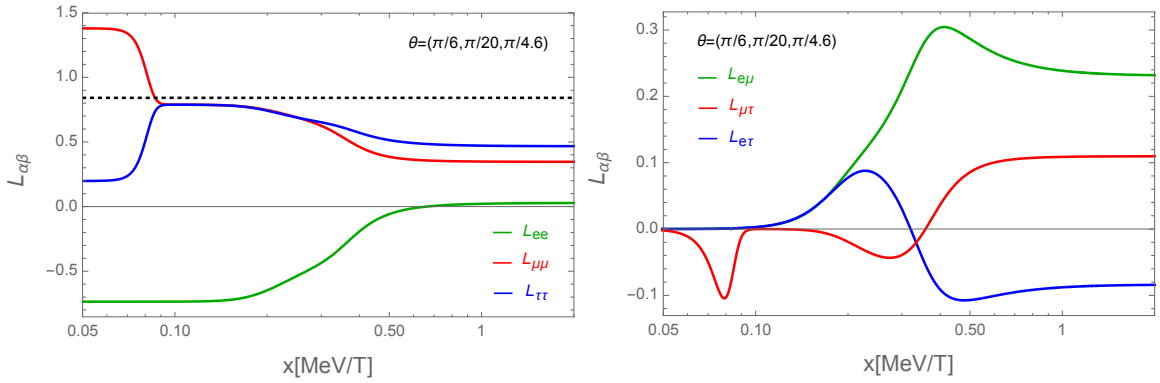

FIG. 1: Evolutions of $\mathbf{L}_{\rm f}$ for $\theta = (\theta_{12}, \theta_{13}, \theta_{23})$ with $(\xi_e, \xi_\mu, \xi_\tau) = (-1, 1.6, 0.3)$. *Left/Right*: Diagonal/off-diagonal entries.

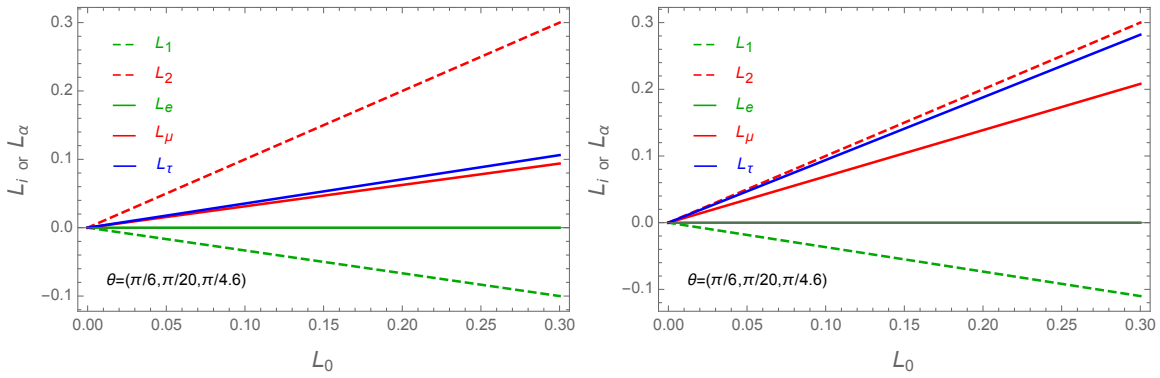

FIG. 2: Comparisons of lepton number asymmetries of both mass-eigenstates (L_i; $i = 1, 2, 3$) and flavor-eigenstates (L_α; $\alpha = e, \mu, \tau$) for $\theta = (\theta_{12}, \theta_{13}, \theta_{23})$ with θ_{ij} being the mixing angles in PMNS matrix. Dashed lines are the asymmetries of mass eigenstates. Solid line are for flavors eigenstates. Left and right panels are showing two examples of $\mathbf{L}_{\rm m}$ leading to $L_e = 0$ satisfying BBN constraint. *Left*: $\mathbf{L}_{\rm m} = {\rm diag}(L_1, L_2, L_3) = (-t_{12}^2 L_0, L_0, 0)$. *Right*: $\mathbf{L}_{\rm m} = {\rm diag}(-(t_{12}^2 + t_{13}^2/c_{12}^2)L_0, L_0, L_0)$.

where $c_{ij}/s_{ij}/t_{ij} = \cos\theta_{ij}/\sin\theta_{ij}/\tan\theta_{ij}$ with θ_{ij} being the mixing angle in PMNS matrix. Since BBN requires $L_e \lesssim \mathcal{O}(10^{-3})$, we may set $L_e = 0$ for an illustration. In this case, L_μ and L_τ are given by

$$\begin{aligned} L_\mu &= c_{23}\left[(1-t_{12}^2)c_{23} - 2s_{13}s_{23}t_{12}\right] L_2 \\ &+ \left[(1-t_{13}^2)s_{23}^2 - t_{12}t_{13}^2 c_{23}(2s_{13}s_{23} + t_{12}c_{23})\right] L_3 \quad (11) \\ L_\tau &= s_{23}\left[(1-t_{12}^2)s_{23} + 2s_{13}c_{23}t_{12}\right] L_2 \\ &+ \left[(1-t_{13}^2)c_{23}^2 - t_{12}t_{13}^2 s_{23}(2s_{13}c_{23} - t_{12}s_{23})\right] L_3 \quad (12) \end{aligned}$$

From Eqs. (11) and (12) with measured values of mixing angles [10], we find that $L_\mu \sim L_\tau$ for $|L_3| \lesssim |L_2|$, as shown in Fig. 2.

COSMOLOGICAL CONSTRAINTS

A large lepton number asymmetry in one or more neutrino species creates an extra radiation density in the universe relative to the standard contributions of photons and CP-symmetric active neutrinos, a form of so-called "dark radiation". Extra relativistic degrees of freedom in cosmology have attracted considerable recent attention as a way to resolve the apparent discrepancy in measurement of the Hubble parameter from CMB data and type-Ia supernovae [9, 18]. In this section, we investigate the possibility that a primordial lepton asymmetry may provide a dark radiation density which can reconcile CMB and SNIa values for the Hubble parameter.

We consider an eight-parameter ΛCDM+ξ cosmology without contribution from primordial tensor fluctuations and assume a normal mass hierarchy for neutrinos, with one massive neutrino with mass $m_\nu = 0.06$ eV. Since the BBN constraint on L_e should be satisfy, we are not free to choose $|L_i| \gg |L_e|$ in an arbitrary way, but constrained to satisfy approximately

$$c_{12}^2 L_1 + s_{12}^2 L_2 + t_{13}^2 L_3 = 0 \quad (13)$$

coming from $L_e = 0$. As the simplest possibility, we may set $L_3 = 0$ leading to $L_1 = -t_{12}^2 L_2$. Then, for thermal distributions of two light mass eigenstates,

$$\begin{aligned}\Delta N_{\rm eff} &= \frac{15}{7}\sum_{i=1,2}\left(\frac{\xi_i}{\pi}\right)^2\left[2+\left(\frac{\xi_i}{\pi}\right)^2\right] \\ &\approx \frac{15}{7}\left(\frac{\xi_2}{\pi}\right)^2 \times \\ &\quad\left\{(1+t_{12}^4)2+\left[1+(4+t_{12}^4)t_{12}^4\right]\left(\frac{\xi_2}{\pi}\right)^2\right\} \quad (14)\end{aligned}$$

where ξ_is are degeneracy parameters of each mass eigenstate, and $|\xi_i| \lesssim 1$ and $t_{12}^2 \ll 1$ were assumed. Strictly speaking, the late-time free-streaming neutrino mass-eigenstates are not in thermal distribution since they are linear combinations of thermal distributions of flavor-eigenstates. Hence, ξ_is in Eq. (14) should be understood as effective degeneracy parameters. The error in $\Delta N_{\rm eff}$ depends on the initial configuration of the lepton number asymmetries in flavor-basis, but it is expected to be of or small than $\mathcal{O}(10)\%$ for $\xi \lesssim 1$.

Figure 3 shows constraints on H_0 and ξ for the case of the eight-parameter ΛCDM+ξ fit. We plot constraints from Planck+BICEP/Keck only (filled contours), and Planck+BICEP/Keck+Riess *et al.* (dotted contours). The CMB data alone show no evidence for nonzero neutrino chemical potential, with a 95%-confidence upper bound of $\xi < 0.53$. For combined CMB and supernova data, there is weak evidence for a nonzero chemical potential, with $\xi = 0.50 \pm 0.19$ at 68% confidence. The combined CMB+supernova data, however, should be interpreted with caution: as the filled contours illustrate, the CMB data and supernova data taken separately are barely compatible, with only a small overlap in the 95% confidence regions, even when dark radiation from a neutrino asymmetry is included as a parameter. Combining two fundamentally incompatible data sets in a Bayesian analysis is likely to give a biased fit, which is reflected in the best-fit values for the two cases, with the best-fit to CMB alone having $-\ln(\mathcal{L}) = 6794.87$, while the best-fit for the the combined CMB+supernova data is measurably worse, with $-\ln(\mathcal{L}) = 6798.47$. For the CMB data alone, including lepton asymmetry, the best-fit Hubble parameter is $H_0 = 67.7 \pm 0.9$, with a 95%-confidence upper bound of $H_0 < 69.7$. This can be compared with a 95%-confidence *lower* bound from Type-Ia supernovae of $H_0 > 69.8$. We therefore conclude, that inclusion of dark radiation from a neutrino asymmetry does not fully reconcile the discrepancy between CMB and supernova data but may be a step in the direction of doing it.

CONCLUSIONS

In this talk, I argued that, when lepton number asymmetries of neutrinos in flavor basis are mixed among themselves due to neutrino oscillation in the early universe before BBN, the asymmetries at the final equilibrium are well described in the basis of mass eigenstates which is related to flavor eigenstates by PMNS matrix. That is, the matrices of lepton number asymmetries in mass- and flavor-basis ($\mathbf{L}_{\rm m}$ and $\mathbf{L}_{\rm f}$, repectively) are related as

$$\mathbf{L}_{\rm m} = U_{\rm PMNS}^{-1}\mathbf{L}_{\rm f}U_{\rm PMNS} \quad (15)$$

where $U_{\rm PMNS}$ is the PMNS matrix, and $\mathbf{L}_{\rm m}$ appears to be diagonal. We demonstrated this argument by a numerical simulation, and showed analytically that the asymmetries of mass-eigenstate can be even larger than those of flavor-eigenstates.

Conventionally, the constraint on the lepton number asymmetries of neutrino flavors has been associated with neutrino flavor-eigenstates, counting their contributions to the extra radiation energy density $\Delta N_{\rm eff}$. However, our argument and finding showed that a proper estimation should be done with neutrino mass-eigenstates in order not to miss the contributions of flavor-mixed states in flavor-basis, and the resulting $\Delta N_{\rm eff}$ can be larger than the one estimated with flavor-eigenstates only.

As shown in Ref. [6–8] and realized in [19] in principle $\Delta N_{\rm eff}$ can be of $\mathcal{O}(0.1-1)$ just from asymmetric neutrinos without resorting to an unknown "dark radiation". Such a large $\Delta N_{\rm eff}$ has been considered in literature as a possible solution to the discrepancy of the measured expansion rate H_0 in CMB and SNIa data. In analyses of cosmological data, typically, if $\Delta N_{\rm eff}$ is from asymmetric neutrinos, the neutrino degeneracy parameters have been taken in an arbitrary way without distinguishing mass- and flavor-eigenstates, although implicitly the lepton number asymmetry (L_e) of electron-neutrinos might be assumed to be small to satisfy BBN constraint. We showed that this approach is inconsistent unless the lepton number asymmetries (L_i) of mass-eigenstates which are relevant for CMB data for example are constrained to satisfy

$$L_e = c_{12}^2 L_1 + s_{12}^2 L_2 + t_{13}^2 L_3 \approx 0 \quad (16)$$

for $|L_e| \lll |L_i|$. Also, analyzing cosmological data (CMB only or CMB+SNIa), we found that CMB data alone show no evidence for nonzero neutrino lepton number asymmetries, with 95% CL upper bound of $|\xi| \lesssim 0.5 - 0.6$ at 95% CL as the degeneracy parameters of two light neutrinos only. For combined CMB and SNIa data, there is weak evidence for nonzero lepton number asymmetries, with $\xi \approx 0.50 \pm 0.19$ at 68% CL, but the fit became worse relative to the case of CMB data alone. So, even if large lepton number asymmetries may fit to the data, it does not look preferred.

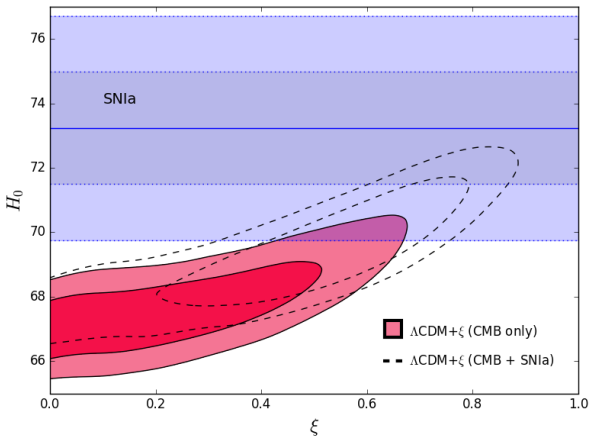

FIG. 3: Constraints on H_0 and ξ for the eight-parameter ΛCDM+ξ case. Filled contours show the 68% (dark red) and 95% (light red) constraints from Planck+BICEP/Keck alone. Dashed contours show the corresponding constraints with the addition of the Riess *et al.* supernova data. The constraint on H_0 from the supernova data alone, $H_0 = 73.24 \pm 1.74$ [18] is shown by the grey filled regions, with 1σ limits in dark grey, and 2σ limits in light grey.

ACKNOWLEDGEMENTS

GB acknowledges support from the MEC and FEDER (EC) Grants SEV-2014-0398 FIS2015-72245-EXP and FPA-2017-84543P and the Generalitat Valenciana under grant PROMETEOII/2013/017.

* Gabriela.Barenboim@uv.es

[1] B. Bajc, A. Riotto and G. Senjanovic, Phys. Rev. Lett. **81**, 1355 (1998) doi:10.1103/PhysRevLett.81.1355 [hep-ph/9710415].

[2] J. Liu and G. Segre, Phys. Lett. B **338**, 259 (1994). doi:10.1016/0370-2693(94)91375-7

[3] J. March-Russell, H. Murayama and A. Riotto, JHEP **9911**, 015 (1999) doi:10.1088/1126-6708/1999/11/015 [hep-ph/9908396].

[4] G. Mangano, G. Miele, S. Pastor, O. Pisanti and S. Sarikas, JCAP **1103**, 035 (2011) doi:10.1088/1475-7516/2011/03/035 [arXiv:1011.0916 [astro-ph.CO]].

[5] G. Mangano, G. Miele, S. Pastor, O. Pisanti and S. Sarikas, Phys. Lett. B **708**, 1 (2012) doi:10.1016/j.physletb.2012.01.015 [arXiv:1110.4335 [hep-ph]].

[6] G. Barenboim and W. I. Park, Phys. Lett. B **765**, 371 (2017) doi:10.1016/j.physletb.2016.12.043 [arXiv:1610.02335 [astro-ph.CO]].

[7] G. Barenboim, W. H. Kinney and W. I. Park, Eur. Phys. J. C **77**, no. 9, 590 (2017) doi:10.1140/epjc/s10052-017-5147-4 [arXiv:1609.03200 [astro-ph.CO]].

[8] G. Barenboim, W. H. Kinney and W. I. Park, Phys. Rev. D **95**, no. 4, 043506 (2017) doi:10.1103/PhysRevD.95.043506 [arXiv:1609.01584 [hep-ph]].

[9] P. A. R. Ade *et al.* [Planck Collaboration], arXiv:1502.01589 [astro-ph.CO].

[10] K. A. Olive *et al.* [Particle Data Group Collaboration], Chin. Phys. C **38**, 090001 (2014). doi:10.1088/1674-1137/38/9/090001

[11] C. Lunardini and A. Y. Smirnov, Phys. Rev. D **64**, 073006 (2001) doi:10.1103/PhysRevD.64.073006 [hep-ph/0012056].

[12] A. D. Dolgov, S. H. Hansen, S. Pastor, S. T. Petcov, G. G. Raffelt and D. V. Semikoz, Nucl. Phys. B **632**, 363 (2002) doi:10.1016/S0550-3213(02)00274-2 [hep-ph/0201287].

[13] Y. Y. Y. Wong, Phys. Rev. D **66**, 025015 (2002) doi:10.1103/PhysRevD.66.025015 [hep-ph/0203180].

[14] K. N. Abazajian, J. F. Beacom and N. F. Bell, Phys. Rev. D **66**, 013008 (2002) doi:10.1103/PhysRevD.66.013008 [astro-ph/0203442].

[15] E. Castorina, U. Franca, M. Lattanzi, J. Lesgourgues, G. Mangano, A. Melchiorri and S. Pastor, Phys. Rev. D **86**, 023517 (2012) doi:10.1103/PhysRevD.86.023517 [arXiv:1204.2510 [astro-ph.CO]].

[16] Z. Maki, M. Nakagawa and S. Sakata, Prog. Theor. Phys. **28**, 870 (1962). doi:10.1143/PTP.28.870

[17] B. Pontecorvo, Sov. Phys. JETP **6**, 429 (1957) [Zh. Eksp. Teor. Fiz. **33**, 549 (1957)].

[18] A. G. Riess *et al.*, Astrophys. J. **826**, no. 1, 56 (2016) doi:10.3847/0004-637X/826/1/56 [arXiv:1604.01424 [astro-ph.CO]].

[19] G. Barenboim and W. I. Park, JCAP **1704**, no. 04, 048 (2017) doi:10.1088/1475-7516/2017/04/048 [arXiv:1703.08258 [hep-ph]].

Non-Abelian Discrete Groups and Neutrino Flavor Symmetry

Morimitsu Tanimoto[1]

Department of Physics, Niigata University, Niigata 950-2181, Japan

Abstract

We discuss the recent progress of flavor models with the non-Abelian discrete symmetry in the lepton sector focusing on the CP violating Dirac phase. It is emphasized that the flavor symmetry with the generalised CP symmetry can predict the CP violating phases.

1 Introduction

The neutrino oscillation experiments have determined precisely the two neutrino mass differences and the three neutrino mixing angles. Especially, the recent data of both T2K and NOνA show that the atmospheric neutrino mixing angle θ_{23} is near the maximal angle 45°. Indeed, the NuFit 3.2 present the best fit $\theta_{23} = 47.2°$ for the normal hierarchy of neutrino masses [1]. The closer maximal mixing $\theta_{23} = 45°$, the more likely that some symmetry behind it. The recent experimental data of T2K and NOνA also strongly indicate the CP violation in the neutrino oscillation [2, 3]. We are in the era to develop the flavor structure of Yukawa couplings by focusing on the leptonic CP violation.

These experimental data give us a big hint of the flavor symmetry. Before the reactor experiments reported the non-zero value of θ_{13}, there was a paradigm of "tri-bimaximal mixing" (TBM) [4, 5], which is a simple mixing pattern for leptons and can be easily derived from flavor symmetries. Some authors succeeded to realize the TBM in the A_4 models [6, 7, 8, 9]. After those successes, the non-Abelian discrete groups are center of attention at the flavor symmetry [10, 11, 12, 13]. The observation of the non-vanishing θ_{13} accelerate the study of flavor models deviating from the TBM [14]. In this talk, we summarize the recent progress of the flavor models with the non-Abelian discrete symmetry.

2 Tri-bimaximal mixing and Flavor symmetry

2.1 Tri-bimaximal mixing

After discovering two large mixing angles of neutrino flavors, Harrison-Perkins-Scott proposed a simple form of the mixing pattern, so-called the tri-bimaximal mixing (TBM) [4, 5] as follows:

$$V_{\rm TBM} = \begin{pmatrix} \frac{2}{\sqrt{6}} & \frac{1}{\sqrt{3}} & 0 \\ -\frac{1}{\sqrt{6}} & \frac{1}{\sqrt{3}} & -\frac{1}{\sqrt{2}} \\ -\frac{1}{\sqrt{6}} & \frac{1}{\sqrt{3}} & \frac{1}{\sqrt{2}} \end{pmatrix} . \tag{1}$$

The TBM is given in the neutrino mass matrix $m_{\nu LL}$

$$m_{\nu LL} = \frac{m_1+m_3}{2}\begin{pmatrix} 1 & 0 & 0 \\ 0 & 1 & 0 \\ 0 & 0 & 1 \end{pmatrix} + \frac{m_2-m_1}{2}\begin{pmatrix} 1 & 1 & 1 \\ 1 & 1 & 1 \\ 1 & 1 & 1 \end{pmatrix} + \frac{m_1-m_3}{2}\begin{pmatrix} 1 & 0 & 0 \\ 0 & 0 & 1 \\ 0 & 1 & 0 \end{pmatrix} , \tag{2}$$

[1] tanimoto@muse.sc.niigata-u.ac.jp

where m_1, m_2 and m_3 are neutrino masses, in the diagonal basis of the charged lepton. It is remarked that the mixing angles are independent of neutrino masses. It is also noticed that this mass matrix is given in terms of integer matrix elements. The non-Abelian symmetry connects different families by taking a doublet or a triplet irreducible representation for three families. The discrete symmetry gives us the definite meaning of three family. Therefore, the non-Abelian discrete symmetry is appropriate for lepton families in the standpoint of the TBM. The third matrix of the r.h.s in Eq.(2) is A_4 symmetric, on the other hand, the first one and the second one are well known as S_3 symmetric. Actually, Ma and Rajasekaran presented a simple model with the A_4 flavor symmetry [6]. After that, many flavor models with the symmetry A_4, A_5, S_3, S_4, D_4, D_6, T', Q_4, Q_6, $\Delta(27)$ or $\Delta(54)$ were proposed.

In 2012, the reactor angle was measured by Daya Bay, Reno and Double Chooz as well as the long-baseline neutrino experiments T2K and MINOS. The mixing angle θ_{13} was found to be of order of the Cabibbo angle, $\theta_c/\sqrt{2} \simeq 9^\circ$, which ruled out the TBM scheme completely. Then, many people worked to explain the deviation from the TBM. In those works, the non-Abelian discrete symmetries have been still active for building flavor models.

2.2 A_4 and S_4 symmetry

The most predictive models involve favor symmetry groups which admit triplet representations. The typical non-Abelian discrete symmetries are A_4 and S_4, which are adopted in some neutrino models.

Let us introduce these groups briefly [11, 12]. All even permutations of four objects form a group, which is called A_4. The order of this group, that is the number of elements, is 12. These elements g are generated by the generators S and T, which satisfy $S^2 = T^3 = (ST)^3 = 1$. They are classified by the conjugacy classes as:

$$\begin{array}{lcll} C_1 & : & \{1\}, & h=1, \\ C_3 & : & \{S, T^2ST, TST^2\}, & h=2, \\ C_4 & : & \{T, ST, TS, STS\}, & h=3, \\ C_4' & : & \{T^2, ST^2, T^2S, ST^2S\}, & h=3, \end{array} \tag{3}$$

where we have also shown the orders of each element in the conjugacy class by h with $g^h = 1$. There are four conjugacy classes and there must be four irreducible representations, **1**, **1′**, and **1″**, and a single triplet **3**.

Next, we present the S_4 group, which consists of all permutations among four objects. The order of S_4 is equal to $4! = 24$. These elements are generated by the generators S, T and U, which satisfy $S^2 = T^3 = U^2 = 1$ and $ST^3 = (SU)^2 = (TU)^2 = 1$. They are classified by the conjugacy classes as:

$$\begin{array}{lcll} C_1 & : & \{1\}, & h=1, \\ C_3 & : & \{S, T^2ST, TST^2\}, & h=2, \\ C_6 & : & \{U, TU, SU, T^2U, STSU, ST^2SU\}, & h=2, \\ C_8 & : & \{T, ST, TS, STS, T^2, ST^2, T^2S, ST^2S\}, & h=3, \\ C_6' & : & \{STU, TSU, T^2SU, ST^2U, TST^2U, T^2STU\}, & h=4. \end{array} \tag{4}$$

The group S_4 includes five conjugacy classes, that is, there are five irreducible representations, two singlets **1** and **1′**, one doublet **2**, and two triplets **3** and **3′**.

2.3 Flavor models with A_4 or S_4 symmetry

The model building of the flavor symmetries is not straightforward since the flavor symmetry group G must be broken. The key of the model building is how the symmetry G is broken. The

predictions depend crucially on the breaking pattern of G. Although G is completely broken in the full theory, there are some relic symmetries of G in the neutrino sector and the charged lepton sector, respectively. These relic symmetries are different in the neutrino sector and the charged lepton sector. This difference is crucial to predict the flavor mixing angles. If no relic symmetries survive, there is no predictive power of the flavor group G.

There are two approaches, the direct one and the indirect one [13]. In the direct approach, the different subgroups of the flavor symmetry survive in the neutrino sector or charged lepton sector. Then, the survival symmetry in the neutrino sector is $Z_2 \times Z_2$ (the Klein symmetry), while the symmetry in the charged lepton sector is Z_3. However, it is not true that the relevant Klein symmetry is a subgroup of the underlying family symmetry G. Indeed, the S_4 group has the relevant subgroup $Z_2 \times Z_2$ which is generated by S and U, but the A_4 symmetry does not.

On the other hand, in the indirect approach, no subgroup of the flavor symmetry survives. Instead, the flavons have special vacuum alignments whose alignment is assisted by the flavor symmetry. These flavons are different ones in the neutrino sector and the charged lepton sector by an additional Z_n symmetry.

2.3.1 Direct Approach of S_4 symmetry

We discuss the direct approach of the $G = S_4$ group. The S_4 group has subgroups, which are nine Z_3, four Z_3, three Z_4 and four $Z_2 \times Z_2$ (Klein four group).

Suppose S_4 is spontaneously broken to one of subgroups, in which

$$K_4 : \{1, S, U, SU\} \ \text{ for neutrinos} , \qquad Z_3 : \{1, T, T^2\} \ \text{ for charged leptons} , \tag{5}$$

are preserved. The neutrino mass matrix $m_{\nu LL}$ respects the S and U generators, on the other hand, the charged lepton mass matrix m_ℓ respects the T generator. Then, these mass matrices satisfy the following relations:

$$S^T m_{\nu LL} S = m_{\nu LL} , \qquad U^T m_{\nu LL} U = m_{\nu LL} , \qquad T^\dagger m_\ell m_\ell^\dagger T = m_\ell m_\ell^\dagger , \tag{6}$$

which turn to

$$[S, m_{\nu LL}] = 0 , \qquad [U, m_{\nu LL}] = 0 , \qquad [T, m_\ell m_\ell^\dagger] = 0 . \tag{7}$$

For the triplets, which are two ones in S_4, the representation of U is taken to be:

$$S = \frac{1}{3}\begin{pmatrix} -1 & 2 & 2 \\ 2 & -1 & 2 \\ 2 & 2 & -1 \end{pmatrix} , \qquad T = \begin{pmatrix} 1 & 0 & 0 \\ 0 & \omega^2 & 0 \\ 0 & 0 & \omega \end{pmatrix} , \qquad U = \mp \begin{pmatrix} 1 & 0 & 0 \\ 0 & 0 & 1 \\ 0 & 1 & 0 \end{pmatrix} , \tag{8}$$

where $\omega^3 = 1$ and the signs $\mp$ in U correspond to the different triplets. The mixing matrix which diagonalizes both S and U is fixed as

$$\begin{pmatrix} 2/\sqrt{6} & 1/\sqrt{3} & 0 \\ -1/\sqrt{6} & 1/\sqrt{3} & -1/\sqrt{2} \\ -1/\sqrt{6} & 1/\sqrt{3} & 1/\sqrt{2} \end{pmatrix} , \tag{9}$$

which is just the TBM mixing matrix. Thus, the TBM is derived from the direct approach of the S_4 group.

There is another possibility of the breaking pattern of the S_4 group. Suppose S_4 is spontaneously broken to

$$Z_2 : \{1, SU\} \ \text{ for neutrinos} , \qquad Z_3 : \{1, T, T^2\} \ \text{ for charged leptons} , \tag{10}$$

preserved. This case is called as the semi-direct approach.

Then, these mass matrices satisfy the following relations

$$[SU, m_{\nu LL}] = 0 \ , \qquad [T, m_\ell m_\ell^\dagger] = 0 \ , \tag{11}$$

which give us another mixing pattern as follows:

$$V_\nu = \begin{pmatrix} 2/\sqrt{6} & c/\sqrt{3} & s/\sqrt{3} \\ -1/\sqrt{6} & c/\sqrt{3} - s/\sqrt{2} & -s/\sqrt{3} - c/\sqrt{2} \\ -1/\sqrt{6} & c/\sqrt{3} + s/\sqrt{2} & -s/\sqrt{3} + c/\sqrt{2} \end{pmatrix} \ , \tag{12}$$

where $c = \cos\phi$ and $s = \sin\phi$ including a CP violating phase. This mixing matrix is also the tri-maximal mixing which is called TM_1.

3 CP symmetry and Flavor Symmetry

Let us start with discussing the generalised CP symmetry [15, 16]. The CP is a discrete symmetry which involves both complex conjugation of the fields and inversion of spatial coordinates,

$$\varphi(x) \to \mathbf{X}_{\mathbf{r_i}} \varphi^*(x') \ , \tag{13}$$

where $x' = (t, -\mathbf{x})$ and $\mathbf{X}_{\mathbf{r_i}}$ is a matrix of transformations of $\varphi(x)$ in the irreducible representation $\mathbf{r_i}$ of the discrete flavor symmetry G. If $\mathbf{X}_{\mathbf{r_i}}$ is the unit matrix, the CP transformation is the trivial one. This is the case for the continuous flavor symmetry [16]. However, in the framework of the discrete family symmetry, non-trivial choices of $\mathbf{X}_{\mathbf{r_i}}$ are possible. The unbroken CP transformation $\mathbf{X}_{\mathbf{r_i}}$s form the group H_{CP}. Then, $\mathbf{X}_{\mathbf{r_i}}$s must be consistent with the flavor symmetry transformation,

$$\varphi(x) \to \rho_{\mathbf{r_i}}(g)\varphi(x) \ , \quad g \in G \ , \tag{14}$$

where $\rho_{\mathbf{r_i}}(g)$ is the representation matrix for g in the irreducible representation $\mathbf{r_i}$.

The consistent condition is obtained as follows. At first, perform a CP transformation $\varphi(x) \to \mathbf{X}_{\mathbf{r_i}}\varphi^*(x')$, then apply a flavor symmetry transformation, $\varphi(x')^* \to \rho_{\mathbf{r_i}}(g)\varphi(x')^*$, and finally an inverse CP transformation. The whole transformation is written as $\varphi(x) \to \mathbf{X}_{\mathbf{r_i}}\rho^*(g)\mathbf{X}_{\mathbf{r_i}}^{-1}\varphi(x)$, which must be equivalent to some flavor symmetry $\varphi(x) \to \rho_{\mathbf{r_i}}(g')\varphi(x)$. Thus, one obtains the consistent condition [17, 18]

$$\mathbf{X}_{\mathbf{r_i}}\rho^*_{\mathbf{r_i}}(g)\mathbf{X}^{-1}_{\mathbf{r_i}} = \rho_{\mathbf{r_i}}(g') \ , \qquad g, g' \in G \ . \tag{15}$$

The full symmetry of the unbroken flavor symmetry and generalised CP symmetry is the semi-direct product of G and H_{CP}, that is $G \otimes H_{CP}$, where G and H_{CP} do not commute in general for the case of the non-Abelian discrete symmetries.

Suppose the full symmetry including the CP symmetry and the flavor symmetry is broken to the subgroups in the neutrino sector and the charged lepton sector, respectively. The CP symmetry gives us the relations as to the neutrino mass matrix and the charged lepton mass matrix as follows:

$$\mathbf{X}^{\nu T}_{\mathbf{r_i}} m_{\nu LL} \mathbf{X}^{\nu}_{\mathbf{r_i}} = m_{\nu LL} \ , \qquad \mathbf{X}^{\ell\dagger}_{\mathbf{r_i}} m_\ell m_\ell^\dagger \mathbf{X}^{\ell}_{\mathbf{r_i}} = m_\ell m_\ell^\dagger \ . \tag{16}$$

Once the subgroups of G and H_{CP} are chosen to satisfy the conditions of Eqs. (15) and (16) for the neutrino sector and the charged lepton sector, respectively, one can predict the CP phase, δ_{CP}.

In this talk, we present an example of the S_4 symmetry [19, 20]. Suppose the full symmetry is broken to G_ν and H^ν_{CP} in the neutrino sector, while the charged lepton sector respects T, that is the diagonal charged lepton mass matrix:

$$G_\nu = \{1, S\}, \qquad X^\nu_{\mathbf{3}} = U, \qquad G_\ell = \{1, T, T^2\}, \qquad X^\ell_{\mathbf{3}} = 1 \ , \tag{17}$$

which satisfy the consistency condition Eq.(15). Then, the neutrino mass matrix, which respects S, is given as

$$m_{\nu LL} = \alpha \begin{pmatrix} 2 & -1 & -1 \\ -1 & 2 & -1 \\ -1 & -1 & 2 \end{pmatrix} + \beta \begin{pmatrix} 1 & 0 & 0 \\ 0 & 0 & 1 \\ 0 & 1 & 0 \end{pmatrix} + \gamma \begin{pmatrix} 0 & 1 & 1 \\ 1 & 1 & 0 \\ 1 & 0 & 1 \end{pmatrix} + \epsilon \begin{pmatrix} 0 & 1 & -1 \\ 1 & -1 & 0 \\ -1 & 0 & 1 \end{pmatrix} \ , \tag{18}$$

where α, β, γ and ϵ are arbitrary complex parameters. Imposing the CP symmetry $S^T m_{\nu LL} S = m^*_{\nu LL}$ in Eq.(16), one finds α, β and γ to be real, and ϵ to be pure imaginary. Then, the neutrino mass in Eq.(18) is diagonalised by the unitary matrix:

$$V_\nu = \begin{pmatrix} 2c/\sqrt{6} & 1/\sqrt{3} & 2s/\sqrt{6} \\ -c/\sqrt{6} + is/\sqrt{2} & 1/\sqrt{3} & -s/\sqrt{6} - ic/\sqrt{2} \\ -c/\sqrt{6} + is/\sqrt{2} & 1/\sqrt{3} & -s/\sqrt{6} + ic/\sqrt{2} \end{pmatrix} \ , \tag{19}$$

where $c = \cos\phi$ and $s = \sin\phi$. Since the charged lepton mass matrix is diagonal, we obtain

$$\sin^2\theta_{13} = \frac{2}{3}\sin^2\phi, \quad \sin^2\theta_{12} = \frac{1}{2+\cos 2\phi}, \quad \sin^2\theta_{23} = \frac{1}{2}, \quad |\sin\delta_{CP}| = 1 \ , \tag{20}$$

which correspond to the maximal CP violation, $\delta_{CP} = \pm\pi/2$. The prediction of the CP phase depends on the respected "Generators" of the flavor symmetry and the CP symmetry. Typically, it is simple values 0, $\pm\pi/2$ or π for other cases [20, 21].

It is useful to summarize the comprehensive work by Chen et al. [18] in the relation between the discrete symmetries and the physical CP invariance guaranteed by generalized CP transformations. They have studied the CP violation by the automorphisms of G carefully. The origin of the CP violation with a discrete flavor symmetry is categorized into three types: (i) Groups explicitly violate CP, which can be related to the complexity of some CG coefficients. An example is the $\Delta(27)$ group. (ii) Groups for which one can find a CP basis in which all the CG coefficients are real. For such groups, imposing CP invariance restricts the phases of coupling coefficients. The examples are A_4, T' and S_4. (iii) Groups that do not admit real CG coefficients, but can define the generalized CP transformation. An example is $\Sigma(72)$.

4 Prospect

The flavor symmetry predicts non-vanishing θ_{13}. The flavor symmetry with the generalised CP symmetry also predicts the CP violating phase. Moreover, the flavor symmetry predicts the mass sum rules. These predictions will be testable by the precise data of the neutrino mixing angles, the CP violating phase and the effective neutrino mass m_{ee}.

On the other hand, we have another important question. Can one predict the CKM mixing matrix in the quark sector from the flavor symmetry? We expect challenging works, in which the neutrino mixing angle θ_{13} is related to the Cabibbo angle and the CP violating phases are related each other in the framework of the unification of quarks and leptons.

Acknowledgement This work is supported by JSPS Grand-in-Aid for Scientific Research 15K05045 and 16H00862.

References

[1] NuFIT 3.2 (2018), www.nu-fit.org.

[2] T2K report, http://t2k-experiment.org/2017/08/t2k-2017-cpv/ , August 4, 2017.

[3] A. Radovic, gLatest oscillation results from NOvA.h Joint Experimental-Theoretical Physics Seminar, Fermilab, USA, January 12, 2018.

[4] P. F. Harrison, D. H. Perkins, W. G. Scott, Phys. Lett. B **530** (2002) 167 [hep-ph/0202074].

[5] P. F. Harrison, W. G. Scott, Phys. Lett. B **535** (2002) 163-169 [hep-ph/0203209].

[6] E. Ma and G. Rajasekaran, Phys. Rev. D **64**, 113012 (2001) [arXiv:hep-ph/0106291].

[7] K. S. Babu, E. Ma and J. W. F. Valle, Phys. Lett. B **552**, 207 (2003) [arXiv:hep-ph/0206292].

[8] G. Altarelli and F. Feruglio, Nucl. Phys. B **720** (2005) 64 [hep-ph/0504165].

[9] G. Altarelli and F. Feruglio, Nucl. Phys. B **741** (2006) 215 [hep-ph/0512103].

[10] G. Altarelli and F. Feruglio, arXiv:1002.0211 [hep-ph].

[11] H. Ishimori, T. Kobayashi, H. Ohki, Y. Shimizu, H. Okada and M. Tanimoto, Prog. Theor. Phys. Suppl. **183** (2010) 1 [arXiv:1003.3552 [hep-th]].

[12] H. Ishimori, T. Kobayashi, H. Ohki, H. Okada, Y. Shimizu and M. Tanimoto, Lect. Notes Phys. **858** (2012) 1, Springer.

[13] S. F. King, A. Merle, S. Morisi, Y. Shimizu and M. Tanimoto, arXiv:1402.4271 [hep-ph].

[14] Y. Shimizu, M. Tanimoto and A. Watanabe, Prog. Theor. Phys. **126** (2011) 81 doi:10.1143/PTP.126.81 [arXiv:1105.2929 [hep-ph]].

[15] G. Ecker, W. Grimus and W. Konetschny, Nucl. Phys. B **191** (1981) 465.

[16] G. C. Branco, R. G. Felipe and F. R. Joaquim, Rev. Mod. Phys. **84** (2012) 515 [arXiv:1111.5332 [hep-ph]].

[17] M. Holthausen, M. Lindner and M. A. Schmidt, JHEP **1304** (2013) 122 [arXiv:1211.6953 [hep-ph]].

[18] M. C. Chen, M. Fallbacher, K. T. Mahanthappa, M. Ratz and A. Trautner, Nucl. Phys. B **883** (2014) 267 [arXiv:1402.0507 [hep-ph]].

[19] F. Feruglio, C. Hagedorn and R. Ziegler, Eur. Phys. J. C **74** (2014) 2753 [arXiv:1303.7178 [hep-ph]].

[20] G. J. Ding, S. F. King, C. Luhn and A. J. Stuart, JHEP **1305** (2013) 084 [arXiv:1303.6180 [hep-ph]].

[21] I. Girardi, A. Meroni, S. T. Petcov and M. Spinrath, JHEP **1402** (2014) 050 [arXiv:1312.1966 [hep-ph]].

Searches for pseudo Nambu-Goldstone Bosons by stimulated resonant photon-photon scatterings with high-intensity laser fields

Kensuke Homma[1]

Graduate School of Science Hiroshima University, 1-3-1 Kagami Yama, Higashi-Hiroshima, Japan 739-8526

Abstract

Pseudo Nambu-Goldstone Bosons (pNGB) can be reasonable candidates for dark components in the universe as long as the coupling to matter fields are weak enough. Because of the lightness of pNGBs, it is possible to directly generate low-mass pNGBs via s-channel resonance scattering by colliding low energy massless particles such as lasers. Laser fields are quite useful due to the huge number of photons per pulse and its coherent nature. The stimulated resonant scattering concept can open up an opportunity to access extremely weak coupling domains as weak as the gravitational coupling strength in much lower mass domains compared to the QCD scale, which have not been intensively explored to date. We present the current status and future prospects based on this novel approach.

1 Introduction

Spontaneous symmetry breaking can be one of the most robust guiding principles to naturally explain dark components in the universe. When a continuous global symmetry is broken, a Nambu-Goldstone Boson (NGB) may appear as a massless particle. In nature, however, an NGB emerges as a pseudo-NGB (pNGB) with a finite mass. Even if a pNGB is close to being massless, its decay into massless particles is kinematically allowed. There are several theoretical models that predict low-mass pNGBs coupling to two photons such as dilatons [1], axions [2], and string-theory-based axion-like particles [3]. These are relevant to dark components of the universe if the coupling to matter fields is weak enough. However, the theoretical evaluation of the physical mass of a pNGB is commonly difficult. Indeed, string theories predict pNGBs to be homogeneously distributed on a log scale in the mass range possibly up to 10^8 eV [3]. Therefore, laboratory tests are necessary to determine the physical masses of pNGBs in a wide mass range. In order to produce pNGBs at an lower center-of-mass (CMS) energy, lower energy colliding beams with massless particles, that is, photon colliders have special roles.

We have previously advocated a novel method [4] for stimulating $\gamma\gamma \to \phi \to \gamma\gamma$ scattering via an s-channel resonant pNGB exchange by utilizing the coherent nature of laser fields. We have first considered a quasi-parallel colliding system (QPS). This colliding system allows us to reach a low CMS energy in the sub-eV range via the small incident angle even if we use a laser field with its photon energy above 1eV. We also have considered an asymmetric-energy head-on collision system (ACS) [5] to access relatively higher CMS energies in order to explain an unidentified emission line, $\omega \sim 3.5$ keV, in the photon energy spectra from a single galaxy and galaxy clusters [6, 7] (the arguments are still actively ongoing [8]) with an interpretation of a pNGB decaying into two photons [9]. This motivated us to extend the same method up to 10 keV by combining different types of coherent and incoherent light sources in ACS [5].

[1]khomma@hiroshima-u.ac.jp

We discuss photon-photon scattering by introducing the following effective Lagrangian in Eq.(1) [4],

$$-L_\phi = gM^{-1}\frac{1}{4}F_{\mu\nu}F^{\mu\nu}\phi, \tag{1}$$

$$-L_\sigma = gM^{-1}\frac{1}{4}F_{\mu\nu}\tilde{F}^{\mu\nu}\sigma, \tag{2}$$

where an effective coupling g/M between two photons and a scalar ϕ or pseudoscalar σ field is introduced. If we are based on the invisible axion scenario [10], a dark field satisfying the dimensional constant $M = 10^{11} - 10^{16}$ GeV and the mass $m =$ meV - μeV can be cold dark matter candidates. If M corresponds to the Planck mass $M_P \sim 10^{18}$ GeV, the interaction is as weak as that of gravity and this case would have a great relevance to explain dark energy if $m \geq$ neV[11].

In this proceedings, we review the basic concept of the proposed method and discuss the future prospect toward direct laboratory searches for pNGBs in the mass range from sub-eV to 10 keV as candidates of the dark components of the universe.

2 Concept of stimulated laser colliders

The proposed method consists of the following two dominant enhancement mechanisms. The first mechanism is the creation of a resonance state via laser-laser collisions by tuning the CMS energy at a pNGB mass, which is the same approach as that in charged particle colliders. The second mechanism is to stimulate the scattering process by adding another background laser field. This feature has never been utilized in high-energy particle colliders, because controllable coherent fields are not available at higher energy scales above 10 keV. We will explain these two mechanisms in the following subsections.

2.1 Inclusion of a resonance state in laser-laser collisions

A CMS energy, E_{cms}, can be generically expressed as

$$E_{cms} = 2\omega \sin\vartheta, \tag{3}$$

where ϑ is defined as a half incident angle between two incoming photons and ω is the beam energy in units of $\hbar = c = 1$. This relation indicates two experimental knobs to adjust E_{cms}. With $\vartheta = \pi/2$, we can realize a CMS head-on collision. A QPS is realized with a small incident angle by focusing a single laser beam, where E_{cms} can be lowered by keeping ω constant. We also consider an asymmetric-energy collision in the head-on geometry in order to relatively increase E_{cms} [5]. Both QPS and ACS correspond to Lorentz boosted systems of CMS. A QPS is realized when a CMS is boosted with respect to the perpendicular direction of head-on collision axis, while a ACS is realized when a CMS is boosted in parallel to the head-on collision axis. Owing to these boosted effects, energies of the final state photons are different from any of incident photon energies. Therefore, frequency shifted photons can be clear signatures of photon-photon scatterings if QPS or ACS are realized as laboratory frames.

We then aim at the direct production of a resonance state via s-channel Feynman amplitude in the photon-photon collisions. The square of the scattering amplitude A proportional to the interaction rate can be expressed as Breit-Wigner resonance function [4]

$$|A|^2 = (4\pi)^2\frac{W^2}{\chi^2(\vartheta) + W^2}, \tag{4}$$

where χ and the width W are defined as $\chi(\vartheta) \equiv \omega^2 - \omega_r^2(\vartheta)$ and $W \equiv (\omega_r^2/16\pi)(g^2m/M)^2$, respectively. The energy ω_r satisfying the resonance condition can be defined as ${\omega_r}^2 \equiv m^2/2(1-\cos 2\vartheta_r)$ [4]. If $\chi^2(\vartheta_r) = 0$ is satisfied, $|A|^2$ approaches to $(4\pi)^2$. This feature is independent of any W in mathematics. However, if $M = M_P$, the width W becomes extremely small. This implies that the resonance width would be too narrow to directly hit the peak of the Breit-Wigner function by any experimental effort. How can we overcome this situation? In a QPS realized in a focused laser field, the incident angles or incident momenta of laser photons become uncertain maximally at the diffraction limit due to the uncertainty principle. This implies that $|A|^2$ must be averaged over the possible uncertainty on E_{cms}. This unavoidable integration over the possible angular uncertainty results in $W \propto 1/M^2$ dependence of $|A|^2$ compared to the $W^2 \propto 1/M^4$ dependence when no resonance is contained in the energy uncertainty, that is, when $\chi^2(\vartheta) \gg W^2$. In ACS too, a similar uncertainty is expected. We have proposed a ACS with high-intensity pulse lasers [5], where the energy uncertainty is caused by the shortness of the pulse duration time via the uncertainty principle again. In both cases the inclusion of a resonance peak enhances the interaction rate by the huge gain factor of M^2.

2.2 Stimulated scattering by coherent laser fields

The inclusion of a resonance state within the uncertainty on E_{cms} is still short in order to reach the sensitivity to the gravitational coupling strength. We thus need an additional enhancement mechanism. We then consider the stimulation of the Feynman amplitude by replacing the vacuum state $|0\rangle$ with the quantum coherent state $|N \gg$ [4]. A laser field is represented by the quantum coherent state which corresponds to a superposition of different photon number states, characterized by the averaged number of photons N [12]

$$|N \gg \equiv \exp(-N/2) \sum_{n=0}^{\infty} \frac{N^{n/2}}{\sqrt{n!}} |n>, \tag{5}$$

where $|n>$ is the normalized state of n photons

$$|n> = \frac{1}{\sqrt{n!}} \left(a^\dagger\right)^n |0>, \tag{6}$$

with $a^\dagger$ and a the creation and the annihilation operators of photons specified with momentum and polarization, respectively. The coherent state satisfies the normalization condition

$$\ll N|N \gg = 1. \tag{7}$$

We can derive following properties of coherent states $|N \gg$ and $\ll N|$:

$$a|N \gg = \sqrt{N}|N \gg \text{ and } \ll N|a^\dagger = \sqrt{N} \ll N| \tag{8}$$

from the familiar relations

$$a^\dagger|n\rangle = \sqrt{n+1}|n+1\rangle \text{ and } a|n+1\rangle = \sqrt{n+1}|n\rangle. \tag{9}$$

The property in Eq.(8) gives the expectation value of the annihilation and creation operators to coherent states

$$\ll N|a|N \gg = \sqrt{N} \text{ and } \ll N|a^\dagger|N \gg = \sqrt{N}. \tag{10}$$

In the production vertex, two incident photons must annihilate from the incident lasers with the momentum p_1 and p_2, respectively. The expectation values associated with the individual

photon legs correspond to the first of Eq.(10). And then if an additional coherent laser field with the momentum p_4 is supplied in advance, the expectation value to create a final state photon p_4 in the sea of the inducing laser field corresponds to the second of Eq.(10). The overall enhancement factor on the interaction rate to have a signal photon with the momentum p_3 is then expressed as

$$(\sqrt{N_{p_1}}\sqrt{N_{p_2}}\sqrt{1_{p_3}}\sqrt{N_{p_4}})^2 = N_{p_1}N_{p_2}N_{p_4}, \tag{11}$$

where N_i indicate the average numbers of photons with momenta p_i. Because N_{p_i} has no limitation due to the bosonic nature of photons, we can expect a huge enhancement factor by the cubic dependence on the photon numbers. This is in contrast to conventional charged particle colliders where the dependence on the number of particles is quadratic and also there is a physical limitation due to the space charge effect. Compared to the upper number of charged particles, typically 10^{11} particles per collision bunch in conventional colliders, Mega Joule laser, for instance, can provide 10 times of Avogadro's number of visible photons per pulse. The cubic nature results in a enormous enhancement factor on the interaction rates. Thus, the stimulated photon collider can provide an extremely high sensitivity to feeble couplings.

3 The current status and future prospect

Figure 1 shows the expected sensitivity by searches in QPS where the search in Hiroshima [13], the search in Kyoto [14], and the prospect at the Romanian Extreme-Light-Infrastructure site (ELI-NP) [15] are shown. We are now in preparation for the search at ELI-NP by forming an international collaboration SAPPHIRES (Search for Axion-like Particle via optical Parametric effects with High-Intensity laseRs in Empty Space) [16] based on the concept introduced here. Figure 2 shows the prospect of sensitivity by searches in ACS. The details of the curves are explained in [5]. In both collision systems, we foresee that the coupling sensitivities can reach the weakness beyond the GUT scale, $M \sim 10^{16}$ GeV, within the currently available laser technology.

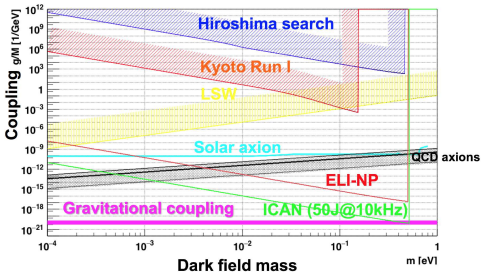

Figure 1: Sensitivity in QPS.

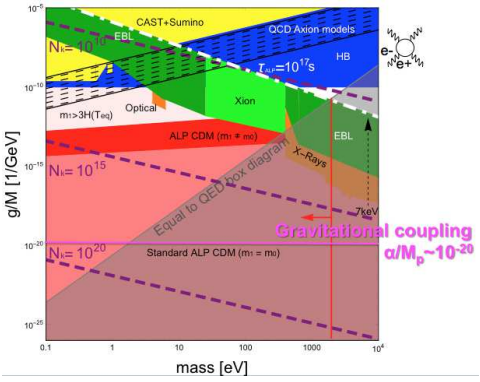

Figure 2: Sensitivity in ACS [5].

Acknowledgements

K. Homma acknowledges the support of the Collaborative Research Program of the Institute for Chemical Research, Kyoto University (Grants Nos. 2017–67 and 2018-83) and the Grants-

in-Aid for Scientific Research Nos. 16H01100, 17H02897 and 18H04354 from MEXT of Japan.

References

[1] Y. Fujii and K. Maeda, *The Scalar-Tensor Theory of Gravitation* Cambridge Univ. Press (2003).

[2] R. D. Peccei and H. R. Quinn, Phys. Rev. Lett **38**, 1440 (1977); S. Weinberg, Phys. Rev. Lett **40**, 223 (1978); F. Wilczek, Phys. Rev. Lett **40**, 271 (1978).

[3] A. Arvanitaki, S. Dimopoulos, S. Dubovsky, N. Kaloper, and J. March-Russell, Phys. Rev. D **81**, 123530 (2010); B. S. Acharya, K. Bobkov, and P. Kumar, J. High Energy Phys. **11**, 105 (2010); M. Cicoli, M. Goodsell, and A. Ringwald, J. High Energy Phys. **10**, 146 (2012).

[4] Y. Fujii and K. Homma, Prog. Theor. Phys **126**, 531 (2011); Prog. Theor. Exp. Phys. 089203 (2014) [erratum].

[5] Kensuke Homma and Yuichi Toyota, Prog. Theor. Exp. Phys. 2017 (2017) no.6, 063C01.

[6] E. Bulbul et al., Astrophys. J. **789**, 13 (2014).

[7] A. Boyarsky, O. Ruchayskiy, D. Iakubovskyi and J. Franse, Phys. Rev. Lett. **113**, 251301 (2014).

[8] E. Bulbul, M. Markevitch, A. Foster, E. Miller, M. Bautz, M. Loewenstein, S. W. Randall and R. K. Smith, Astrophys. J. **831**, 55 (2016) ; F. A. Aharonian *et al.* [Hitomi Collaboration], arXiv:1607.07420 [astro-ph.HE] ; J. P. Conlon, F. Day, N. Jennings, S. Krippendorf and M. Rummel, arXiv:1608.01684 [astro-ph.HE].

[9] J. Jaeckel, J. Redondo and A. Ringwald, Phys.Rev. D **89**, 103511 (2014).

[10] Mark P. Hertzberg, Max Tegmark, and Frank Wilczek, Phys. Rev. D **78**, 083507 (2008); O. Wantz and E. P. S. Shellard, Phys. Rev. D 82, 123508 (2010).

[11] Y. Fujii and K. Maeda, *The Scalar-Tensor Theory of Gravitation* Cambridge Univ. Press (2003).

[12] R. J. Glauber, Phys. Rev. **131** (1963), 2766.

[13] K. Homma, T. Hasebe, and K.Kume, Prog. Theor. Exp. Phys. 083C01 (2014).

[14] T. Hasebe, K. Homma, Y. Nakamiya, K. Matsuura, K. Otani, M. Hashida, S. Inoue, S. Sakabe, Prog. Theor. Exp. Phys. 073C01 (2015).

[15] K. Homma, O. Tesileanu, L. D'Alessi, T. Hasebe, A. Ilderton, T. Moritaka, Y. Nakamiya, K. Seto, H. Utsunomiya, Y. Xu, Romanian Reports in Physics, Vol. 68, Supplement, P. S233-S274 (2016).

[16] http://home.hiroshima-u.ac.jp/spphrs/

Relation of CLFV to cosmological observables in the CMSSM coannihilation scenario with SeeSaw mechanism

Masato Yamanaka[1]

Maskawa Institute, Kyoto Sangyo University, Kyoto 603-8555, Japan

Abstract

We investigate the constrained minimal supersymmetric standard model with three right-handed Majorana neutrinos whether there still is a parameter region which is consistent with all existing experimental data/limits such as leptogenesis and the dark matter abundance and we also can solve the Lithium problem. We study three cases of the right-handed neutrino mass ratio (i) $M_2 = 2 \times M_1, M_3 = 40 \times M_1$, (ii) $M_2 = 4 \times M_1, M_3 = 40 \times M_1$, (iii) $M_2 = 10 \times M_1, M_3 = 40 \times M_1$. We obtain the mass range of the lightest right-handed neutrino mass that lies between 10^9 GeV and 10^{10} GeV. The important result is that its upper limit is derived by solving the Lithium problem and the lower limit comes from leptogenesis. Low-energy observables of these parameter sets such as BR($\mu \to e\gamma$) will be verified in the near future. This talk is based on Ref. [1].

1 Introduction

There are several phenomena which cannot be explained by the standard models (SMs) of particle physics and cosmology. Among such phenomena, the mass and mixing of neutrinos, the Baryon asymmetry of the universe (BAU), the existence of the dark matter (DM), so-called Lithium (Li) problems are compelling evidences that require new physics for explanations. The new physics should be incorporated in a unified picture beyond the SM of particle physics.

Supersymmetry (SUSY) with R parity is an attractive extension, where the lightest SUSY particle (LSP) become stable. In many SUSY models, the LSP is the lightest neutralino, and is a candidate for the DM. A most feasible parameter region where the neutralino relic density is consistent with the observed DM density is the so-called coannihilation region, in which the neutralino DM and the lighter stau, as the next-LSP (NLSP), are degenerate in mass [2].

When the mass difference of the neutralino and the stau is smaller than tau lepton mass, the stau becomes long-lived so that it can survive during the Big-Bang nucleosynthesis (BBN) proceeds [3]. Such a long-lived stau forms a bound state with light nuclei, and induces some kinds of exotic nuclear reactions. Disagreements between predicted and observed primordial abundances for ^{6}Li and ^{7}Li are so-called Li problems [4, 5], and could be solved via the exotic reactions [6, 7, 8].

How about the neutrino mass and the BAU? The neutralino-stau coannihilation scenario successfully accounts for the DM and solve the problems of BBN. If the scenario actually describes our universe, tiny neutrino masses and the observed baryon asymmetry also must be generated in this scenario. In this work, we consider the constrained minimal supersymmetric standard model (CMSSM) with the type I seesaw mechanism as a unified picture. We quantitatively search for the parameter space where all phenomena as we have mentioned above are successfully explained, and will show characteristic observables for this scenario.

2 Cosmological constraints

We take into account three cosmological observables; *(i)* DM abundance *(ii)* light element abundances *(iii)* baryon asymmetry. We show strategy to find favored parameter space. We

[1]masato.yamanaka@cc.kyoto-su.ac.jp

consider the neutralino-slepton coannihilation scenario where the LSP is Bino-like neutralino $\widetilde{\chi}_1^0$ and NLSP is lightest slepton that almost consist of RH stau including tiny flavor mixing, $\widetilde{\ell}_1 = \sum_{f=e,\mu,\tau} C_f \widetilde{f}$. The interaction state is $\widetilde{f} = \cos\theta_f \widetilde{f}_L + \sin\theta_f \widetilde{f}_R$. The flavor mixing C_f and left-right mixing θ_f are determined by RG equations with neutrino Yukawa.

In a unique parameter space for the neutralino-slepton coannihilation, we focus on the space where the mass difference between $\widetilde{\chi}_1^0$ and $\widetilde{\ell}_1$ is smaller than tau mass. Assuming flavor conservation, open decay channels of $\widetilde{\ell}_1$ are $\widetilde{\ell}_1 \to \widetilde{\chi}_1^0 \nu_\tau \pi$, $\widetilde{\ell}_1 \to \widetilde{\chi}_1^0 \nu_\tau \ell \bar{\nu}_\ell$ $(\ell \ni e, \mu)$, and so on. Due to the phase space suppression and higher order coupling the $\widetilde{\ell}_1$ becomes a long-lived particle [9, 3]. If the lepton flavor is violated, the 2-body decays are allowed, $\widetilde{\ell}_1 \to \widetilde{\chi}_1^0 \ell$ $(\ell \ni e, \mu)$. Thus the longevity depends on the degeneracy in mass and also on the magnitude of LFV.

The long-lived $\widetilde{\ell}_1$ has significant effect on light element abundances through exotic nuclear processes. To quantitatively see this effect, we evaluate the $\widetilde{\ell}_1$ number density on the BBN era.

2.1 Dark matter relic density

After SUSY particles ($\widetilde{\chi}_1^0$ and $\widetilde{\ell}_1$) are chemically decoupled from SM sector, their total density, $n = n_{\widetilde{\chi}_1^0} + n_{\widetilde{\ell}_1^-} + n_{\widetilde{\ell}_1^+}$, will be frozen. Since all of SUSY particles eventually decays into the LSP, the DM relic density is indeed the total density. We search for favored parameters by numerically solving the equation to fit n to the observed DM density [10], $0.1133 \leq m_{\widetilde{\chi}_1^0} n h^2/\rho_c \leq 0.1265$ (3σ C.L.), where $h = 0.673$ is the Hubble constant normalized to $H_0 = 100\,\mathrm{km\,s^{-1}\,Mpc^{-1}}$, and $\rho_c = 1.054 \times 10^{-5}\,\mathrm{GeV\,cm^{-3}}$ is the critical density of the universe.

2.2 Number density of long-lived slepton

Even after the chemical decoupling, although the total density remains the current DM density, each number density of $\widetilde{\chi}_1^0$, $\widetilde{\ell}_1^-$, and $\widetilde{\ell}_1^+$ continues to evolve. As long as the kinetic equilibrium with the SM sector is maintained, $\widetilde{\ell}_1$ and $\widetilde{\chi}_1^0$ follow the Boltzmann distribution. Processes maintaining the kinetic equilibrium are $\widetilde{\ell}_1^\pm \gamma \leftrightarrow \widetilde{\chi}_1^0 \tau^\pm$, $\widetilde{\ell}_1^\pm \tau^\mp \leftrightarrow \widetilde{\chi}_1^0 \gamma$, and so on. Even for a tiny LFV, flavor changing processes are relevant due to much larger densities of e and μ compared with of τ for the universe temperature smaller than m_τ. For example, for a reference universe temperature $T = 70\,\mathrm{MeV}$, reaction rates of these processes are

$$\frac{\langle \sigma' v \rangle_{\widetilde{\ell}_1 e \leftrightarrow \widetilde{\chi}_1^0 \gamma} n_e}{\langle \sigma' v \rangle_{\widetilde{\ell}_1 \tau \leftrightarrow \widetilde{\chi}_1^0 \gamma} n_\tau} \simeq \left(1.08 \times 10^9\right) C_e^2\,, \quad \frac{\langle \sigma' v \rangle_{\widetilde{\ell}_1 \mu \leftrightarrow \widetilde{\chi}_1^0 \gamma} n_\mu}{\langle \sigma' v \rangle_{\widetilde{\ell}_1 \tau \leftrightarrow \widetilde{\chi}_1^0 \gamma} n_\tau} \simeq \left(9.93 \times 10^7\right) C_\mu^2\,. \tag{1}$$

As long as $C_e \gtrsim 3.2 \times 10^{-5}$ and $C_\mu \gtrsim 1.0 \times 10^{-4}$, flavor changing processes maintain the kinetic equilibrium, and hence reduce $n_{\widetilde{\ell}_1^-}$.

2.3 Leptogenesis

We calculate the lepton asymmetry assuming the RH neutrinos being hierarchical in mass. Typical parameters for solving the Li problems are $M_1 \sim 10^{10}\,\mathrm{GeV}$ and $|\lambda_{\alpha 1}| \sim 10^{-3}$. Further, the decay parameter should be $K \equiv \Gamma_{N_1}/H(M_1) \sim \mathcal{O}(1)$ and $K_\alpha \equiv K \cdot \mathrm{BR}(N_1 \to \ell_\alpha \phi) \sim \mathcal{O}(0.1)$ $(\alpha \ni e, \mu, \tau)$. Here $H(M_1)$ is the Hubble parameter at $T = M_1$. Under such conditions, the lepton number of each flavor separately evolves, and it gives rise to $\mathcal{O}(1)$ corrections to the final lepton asymmetry with respect to where the flavor effects are ignored. The lepton and slepton asymmetry converts to the baryon asymmetry, and the conversion factor in MSSM scenarios is $Y_B = (8/23) Y_{B-L}$. The required lepton asymmetry in 3 sigma range is $2.414 \times 10^{-10} \lesssim |Y_{B-L}| \lesssim 2.561 \times 10^{-10}$ for the observed baryon number $\Omega_b h^2 = 0.0223 \pm 0.0002$ (1σ).

3 Analysis and Summary

Fig. 1 shows the correlation between M_1 and the branching ratio of $\mu \to e\gamma$ depending on M_2. The reaction rate displayed is basically proportional to the second lightest Majorana neutrino mass M_2. The enhancement comes from the elements of the Dirac neutrino Yukawa matrix λ_ν that have large absolute values for a fixed active neutrino parameter $|(\lambda_\nu)_{i2}| \propto M_2$. Each line possesses start and end point. The ^{7}Li problem is solved throughout each line. While the region wherein both ^{7}Li and ^{6}Li problems are solved is limited on the thick part in each line. It is easily understood. Too large M_1 gives rise to too large slepton mixing, and the long-lived slepton decays via the mixing before forming a bound state with ^{4}He.

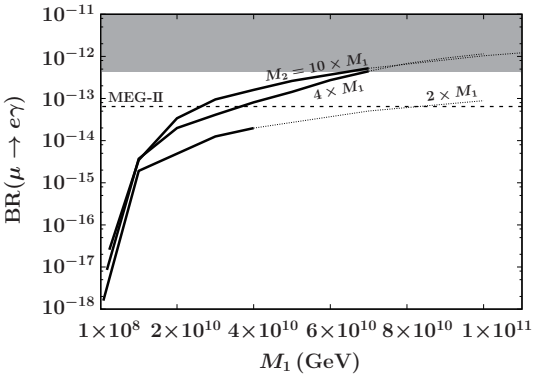

Figure 1: $\mathrm{BR}(\mu \to e\gamma)$ as a function of M_1 for $M_2 = 2 \times M_1$, $4 \times M_1$, and $10 \times M_1$. Both the ^{7}Li and ^{6}Li problems are solved with parameters for thick part, while only the ^{7}Li problem is solved for thin part. Gray region is excluded region, and the horizontal line show future sensitivity.

The parameter of RH neutrino is narrowed down to a small space through solving the ^{7}Li/^{6}Li problems and generating lepton asymmetry. This parameter leads to the clear correlation, which is therefore one of the characteristic prediction of this scenario. The prediction for $\mathrm{BR}(\mu \to e\gamma)$ lies in the range where the recent and near future experiment can probe. Our scenario can be precisely illuminated by combining LFV observables and unique collider signals.

Acknowledgement The author would like to thank organizers for financial support for traveling and local expenses.

References

[1] M. Kubo, J. Sato, T. Shimomura, Y. Takanishi and M. Yamanaka, arXiv:1803.07686.

[2] K. Griest and D. Seckel, Phys. Rev. D **43** (1991) 3191.

[3] T. Jittoh, J. Sato, T. Shimomura and M. Yamanaka, Phys. Rev. D **73** (2006) 055009.

[4] R. H. Cyburt, B. D. Fields and K. A. Olive, JCAP **0811** (2008) 012.

[5] M. Asplund, D. L. Lambert, P. E. Nissen, F. Primas and V. V. Smith, Astrophys. J. **644** (2006) 229.

[6] M. Pospelov, Phys. Rev. Lett. **98** (2007) 231301.

[7] T. Jittoh, K. Kohri, M. Koike, J. Sato, T. Shimomura and M. Yamanaka, Phys. Rev. D **76** (2007) 125023.

[8] C. Bird, K. Koopmans and M. Pospelov, Phys. Rev. D **78** (2008) 083010.

[9] S. Profumo, K. Sigurdson, P. Ullio and M. Kamionkowski, Phys. Rev. D **71** (2005) 023518.

[10] C. Patrignani *et al.* [Particle Data Group], Chin. Phys. C **40** (2016) no.10, 100001.

Towards the minimal seesaw model for the prediction of neutrino CP violaion

Yusuke Shimizu[a 1] , Kenta Takagi[a 2] , Morimitsu Tanimoto[b 3]

[a] *Graduate School of Science Hiroshima University, Higashi-Hiroshima 739-8526, Japan*

[b] *Department of Physics, Niigata University, Niigata 950-2181, Japan*

Abstract

We discuss the minimal seesaw model for the Dirac CP violating phase of the lepton mixing matrix. We introduce two right-handed Majorana neutrinos and obtain several textures of the tri-maximal lepton mixing matrices. Moreover, we discuss the observed baryon asymmetry of the universe through the leptogenesis mechanism. As the result, we obtain the specific model which predicts the negative sign of maximal Dirac CP violating phase and normal hierarchy of neutrino masses.

1 Our minimal seesaw model

The remarkable developments in the neutrino oscillation experiments fuel our expectations for the future discovery of CP violation in the lepton sector. Indeed, recent T2K data strongly indicate the CP violation [1]. In order to discuss the theoretical aspects of the CP violation in the lepton sector, we investigate the minimal seesaw model via the CP violation and baryon asymmetry of the universe (BAU). Here, we briefly explain how to build our minimal seesaw model.

- The minimal seesaw model includes two heavy right-handed Majorana neutrinos and three left-handed neutrinos in Type I seesaw [2]. We take both the charged lepton and right-handed Majorana neutrino mass matrix M_R to be real diagonal. M_R and the Dirac neutrino mass matrix M_D are generally written as

$$M_R = -M_2 \begin{pmatrix} p^{-1} & 0 \\ 0 & 1 \end{pmatrix}, \quad M_D = \begin{pmatrix} a & d \\ b & e \\ c & f \end{pmatrix}, \quad p = M_2/M_1 \tag{1}$$

  the neutrino mass matrix is obtained by the Type I seesaw:

$$M_\nu = -M_D M_R^{-1} M_D^T = \frac{1}{M_0} \begin{pmatrix} a^2p + d^2 & abp + de & acp + df \\ abp + de & b^2p + e^2 & bcp + ef \\ acp + df & bcp + ef & c^2p + f^2 \end{pmatrix}. \tag{2}$$

- We consider the lepton mixing matrix in the two frameworks of tri-maximal mixing, TM_1 and TM_2 which are derived from additional rotation of 2-3 and 1-3 plane to the tri-bi-maximal lepton mixing [3, 4] respectively. The following textures of Dirac neutrino mass matrices realize the tri-maximal lepton mixing:

[1] yu-shimizu@hiroshima-u.ac.jp
[2] takagi-kenta@hiroshima-u.ac.jp
[3] tanimoto@muse.sc.niigata-u.ac.jp

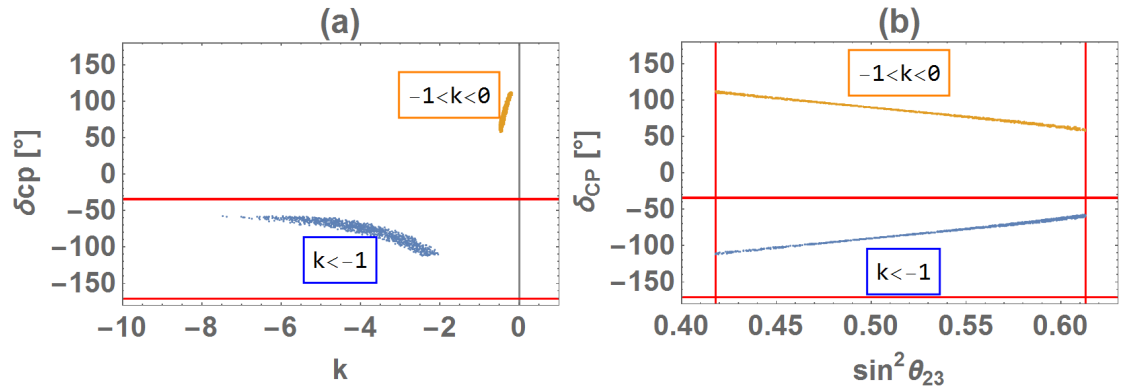

Figure 1: Predictions in case I, where the blue and orange dots denote the region of $k < -1$ and $-1 < k < 0$. The red lines for $\sin^2\theta_{23}$ and δ_{CP} denote the experimental bounds of 3σ (global analyses) and 2σ (T2K) ranges, respectively: (a) δ_{CP} versus k, (b) δ_{CP} versus $\sin^2\theta_{23}$.

$$M_D = \begin{pmatrix} \frac{b+c}{2} & \frac{e+f}{2} \\ b & e \\ c & f \end{pmatrix}, \quad \begin{pmatrix} -2b & \frac{e+f}{2} \\ b & e \\ b & f \end{pmatrix}, \quad \begin{pmatrix} b & -(e+f) \\ b & e \\ b & f \end{pmatrix}, \tag{3}$$

where they realize TM_1 for normal hierarchy (NH), TM_1 for inverted hierarchy (IH) and TM_2 for either NH or IH of neutrino masses respectively.

- We can discuss the BAU through the leptogenesis mechanism [5] in the decay of lighter right-handed neutrino M_1 only for the TM_1 with NH texture since only this texture produces the finite interference term between tree and 1 loop diagrams of the M_1 decay.

Therefore, we focus on the texture of TM_1 with NH in the following. In order to minimize our model, we impose zero in this texture. The following three types of Dirac neutrino mass matrices are possible.

$$M_D^{\mathrm{I}} = \begin{pmatrix} 0 & \frac{e+f}{2} \\ b & e \\ -b & f \end{pmatrix}, \quad M_D^{\mathrm{II}} = \begin{pmatrix} \frac{b}{2} & \frac{e+f}{2} \\ b & e \\ 0 & f \end{pmatrix}, \quad M_D^{\mathrm{III}} = \begin{pmatrix} \frac{c}{2} & \frac{e+f}{2} \\ 0 & e \\ c & f \end{pmatrix} \tag{4}$$

2 Numerical analysis

We discuss the correlation between the predicted CP violating phase δ_{CP} and the BAU through the leptogenesis. Our analysis about the leptogenesis mainly follows a simple framework [6] which is valid under the condition, $M_1 \ll M_2$ and $M_1 \ll 10^{14}$[GeV].

Here, we discuss the numerical results of TM_1 with NH. We use the recent neutrino oscillation data from NuFIT 3.2 (2018) [7] for the input data. According to this global experimental data, the numerical results from M_D^{II} and M_D^{III} are excluded from 3σ C.L.. Therefore, we only show the results of M_D^{I} in Figure 1. The results reflect the constraint from not only the recent neutrino oscillation data but also the observed BAU, $\eta_B \simeq [5.8, 6.6] \times 10^{-10}$ 95%C.L. [8]. These predictions are calculated in the case of $M_2 = 10^{14}$GeV. But the correlations in Figure 1 are independent of M_2. We note that the ratio of right-handed neutrino masses $p = M_2/M_1$ is allowed ,roughly speaking, within $p = [200 \sim 300]$ ($p = [2000 \sim 3000]$) for $M_2 = 10^{14}$[GeV] ($M_2 = 10^{15}$[GeV]).

Let's discuss the left panel of Figure 1. We show the $k = e/f$ dependence of the predicted δ_{CP} by inputting the observed BAU. It is remarked that δ_{CP} is predicted to be negative for $k < -1$ while it is positive for $-1 < k < 0$. The negative and maximal CP violation $\delta_{CP} \sim -\pi/2$ is realized around $k \sim -3$.

In the right panel of Figure 1, we show the predicted correlation between δ_{CP} versus $\sin^2\theta_{23}$. It indicates an important feature of this model: The maximal CP violation and mixing angle $(\delta_{CP}, \theta_{23}) = (-\pi/2, \pi/4)$ can be realized for $k < -1$ simultaneously, which is favored if we take account of the current data and future prospects.

3 Summary and discussions

We have studied the correlation between the CP violating phase δ_{CP} and the observed BAU in the minimal seesaw model, where two right-handed Majorana neutrinos are assumed. We have also taken the tri-maximal mixing pattern for the neutrino flavor (TM_1 or TM_2) in the diagonal basis of both the charged lepton and right-handed Majorana neutrino mass matrices. We have found the clear correlation between the CP violating phase δ_{CP} and BAU for TM_1 in NH of neutrino masses. The parameter k should be smaller than -1 in order to predict a negative δ_{CP}, which is indicated by the recent T2K data. It is emphasized that our Dirac neutrino mass matrix predicts the negative sign of δ_{CP} and the observed value of BAU as far as we take $k < -1$ under the condition, $M_1 \ll M_2$.

Acknowledgement This work is supported by JSPS Grants-in-Aid for Scientific Research 16J05332 (YS) and 15K05045, 16H00862 (MT).

References

[1] T2K report, http://t2k-experiment.org/2017/08/t2k-2017-cpv/, August 4, 2017.

[2] Y. Shimizu, R. Takahashi and M. Tanimoto, PTEP **2013** (2013) no.6, 063B02 [arXiv:1212.5913 [hep-ph]].

[3] P. F. Harrison, D. H. Perkins, W. G. Scott, Phys. Lett. B **530** (2002) 167 [hep-ph/0202074].

[4] P. F. Harrison, W. G. Scott, Phys. Lett. B **535** (2002) 163-169 [hep-ph/0203209].

[5] M. Fukugita and T. Yanagida, Phys. Lett. B **174** (1986) 45.

[6] G. F. Giudice, A. Notari, M. Raidal, A. Riotto and A. Strumia, Nucl. Phys. B **685** (2004) 89 [hep-ph/0310123].

[7] NuFIT 3.2 (2018), www.nu-fit.org/

[8] C. Patrignani *et al.* [Particle Data Group], Chin. Phys. C **40** (2016) no.10, 100001.

The full references are available in [arXiv:1709.02136] and [arXiv:1711.03863].

Enhanced axion photon coupling in GUT with hidden photon

Norimi Yokozaki

Department of Physics, Tohoku University,
Sendai, Miyagi 980-8578, Japan

Abstract

We show that the axion-photon coupling is enhanced, if the gauge coupling unification is realized by a large kinetic mixing $\chi = \mathcal{O}(0.1)$ between $\mathrm{U}(1)_Y$ and unbroken hidden $\mathrm{U}(1)_H$. The key ingredient is that the $\mathrm{U}(1)_H$ gauge coupling should be rather large to induce large χ, leading to enhanced contributions to the electromagnetic anomaly from hidden matter fields. We find that the axion-photon coupling is enhanced by about a factor of 10 - 100 with respect to the GUT-axion models with $E/N = 8/3$.

1 Introduction

The axion, a, is a pseudo-Nambu-Goldstone boson associated with spontaneous breakdown of a global $\mathrm{U}(1)_{\mathrm{PQ}}$ symmetry in the Peccei-Quinn (PQ) mechanism [1–4]. The axion provides not only a solution to the strong CP problem but also an explanation for the observed dark matter [5–7].

The axion has been searched for by numerous experiments (see e.g. Refs. [8,9] for recent reviews). Many of the on-going and planned experiments utilize the axion-photon coupling,

$$\mathcal{L} = \frac{g_{a\gamma\gamma}}{4} a F_{\mu\nu} \tilde{F}^{\mu\nu}, \tag{1}$$

where $F_{\mu\nu}$ is the photon field strength, and $\tilde{F}^{\mu\nu}$ denotes its dual. Therefore, the size of the axion-photon coupling $g_{a\gamma\gamma}$ is a very important input for such experiments.

Another important motivation for physics beyond the standard model (SM) is grand unified theories (GUTs). In a non-supersymmetric GUT, however, the unification scale tends to be too low to satisfy the proton decay constraint. Moreover, the gauge couplings fail to unify at a single scale. One of the remedies for the gauge coupling unification is to add a massless hidden photon which has a large kinetic mixing with hypercharge, $\mathrm{U}(1)_Y$ [10]. According to the recent analysis using the two-loop renormalization group (RG) equations [11], the unification scale is shown to be at $10^{16.5}\,\mathrm{GeV}$ and the required kinetic mixing is $\chi(m_Z) \approx 0.37$. Interestingly, the unification with a hidden photon is rather robust against adding visible or hidden matters [11,12]. This finding enables us to incorporate the axion into the framework in a consistent manner.

Here, we study the axion-photon coupling in a GUT scenario where a massless hidden photon has a large kinetic mixing with $\mathrm{U}(1)_Y$. Since the kinetic mixing between $\mathrm{U}(1)_Y$ and $\mathrm{U}(1)_H$ is induced by one-loop diagrams with bi-charged particles running in the loop, it requires rather strong hidden $\mathrm{U}(1)_H$ gauge coupling [11, 12]. As we shall see, the large kinetic mixing and strong $\mathrm{U}(1)_H$ gauge coupling enhance the electromagnetic anomaly, and the axion coupling to photons can be enhanced. Such enhancement is advantageous for the axion search experiments utilizing the the axion photon coupling.

2 Axion coupling to photons and kinetic mixing

First, let us briefly review the standard case without $\mathrm{U}(1)_H$. We introduce a single complex scalar field ϕ to break the global $\mathrm{U}(1)_{\mathrm{PQ}}$ symmetry spontaneously. The potential for ϕ is given by

$$V = \lambda_{PQ} \left(|\phi|^2 - \frac{v_{PQ}^2}{2} \right)^2, \tag{2}$$

with $\lambda_{PQ} > 0$, and ϕ contains the axion in its phase component:

$$\phi = \frac{v_{PQ} + \rho(x)}{\sqrt{2}} \exp\left(i\frac{a(x)}{v_{PQ}}\right). \tag{3}$$

The field $\rho(x)$ has a large mass around v_{PQ}, and it is irrelevant for our discussion.

The global $\mathrm{U(1)_{PQ}}$ symmetry is assumed to be explicitly broken by the QCD anomaly. For this purpose, one introduces heavy PQ fermions, $\psi_L^{(i)}$ and $\psi_R^{(i)}$, which couple to ϕ as

$$\sum_i \phi\, \bar{\psi}_L^{(i)} \psi_R^{(i)} + \text{h.c.} \tag{4}$$

Here and in what follows we assign PQ charges 1 and 0 on $\psi_L^{(i)}$ and $\psi_R^{(i)}$, respectively. The PQ fermions include PQ quarks charged under $\mathrm{SU(3)}_C$. Through one-loop diagrams involving the PQ quarks, the axion couples to gluons as

$$\frac{g_s^2}{32\pi^2 f_a} a\, G^a_{\mu\nu} \tilde{G}^{a\mu\nu}, \tag{5}$$

where $G^a_{\mu\nu}$ is the gluon field strength, $\tilde{G}^{a\mu\nu}$ is its dual, and $f_a = v_{PQ}/N_{DW}$ is the decay constant of the QCD axion. In the above case, N_{DW} is equal to the number of the heavy PQ quarks. The axion acquires a mass due to topological fluctuations of the gluon fields in QCD [13],

$$m_a = 5.70(7)\,\mu\text{eV}\left(\frac{10^{12}\,\text{GeV}}{f_a}\right). \tag{6}$$

which is inversely proportional to f_a.

In general, the QCD axion also couples to photons through the electromagnetic anomaly and mixings with neutral mesons. The axion-photon coupling $g_{a\gamma\gamma}$ in Eq.(1) is given by [13]

$$g_{a\gamma\gamma} = \frac{\alpha_{\text{EM}}}{2\pi f_a}\left(\frac{E}{N} - 1.92(4)\right), \tag{7}$$

where α_{EM} is the fine-structure constant, and E and N are the electromagnetic and color anomaly coefficients given by

$$E = \sum_i (Q^{(i)}_{\text{EM}})^2 Q^{(i)}_{\text{PQ}}, \quad N\delta_{ab} = \sum_i \text{Tr}\lambda_a\lambda_b Q^{(i)}_{\text{PQ}}, \tag{8}$$

where $Q^{(i)}_{\text{EM}}$ is the electric charge of $\psi^{(i)}$, $Q^{(i)}_{\text{PQ}}$ the PQ charge of $\psi_L^{(i)}$, λ_a the generators for the PQ quarks under SU(3). For the fundamental representation of $\mathrm{SU(3)}_C$, we have $N = \frac{1}{2}\sum Q_{\text{PQ}}$. The ratio of the electromagnetic and color anomaly coefficients, E/N, is equal to 8/3 if the PQ fermions form complete multiplets under $\mathrm{SU(5)_{GUT}}$, and equal to 0 if the PQ fermions do not carry any electric charges. So the axion-photon coupling is determined by the gauge coupling constant and the anomaly coefficient.

Next, we consider the effect of $\mathrm{U(1)}_H$ and its kinetic mixing with $\mathrm{U(1)}_Y$. In the original basis where the kinetic mixing is present, the kinetic terms of the hypercharge and hidden gauge bosons, $A'_{Y\mu}$ and $A'_{H\mu}$, are

$$\mathcal{L}_K = -\frac{1}{4}F'^{\mu\nu}_Y F'_{Y\mu\nu} - \frac{1}{4}F'^{\mu\nu}_H F'_{H\mu\nu} - \frac{\chi}{2}F'^{\mu\nu}_Y F'_{H\mu\nu}, \tag{9}$$

where $F'_{\mu\nu}$ and $F'_{H\mu\nu}$ are field strengths of $\mathrm{U(1)}_Y$ and $\mathrm{U(1)}_H$, respectively. Let us introduce a PQ fermion $\psi(q_Y, q_H)$ charged under $\mathrm{U(1)}_Y$ and $\mathrm{U(1)}_H$. The relevant part of the Lagrangian is

$$\begin{aligned} \mathcal{L}_\psi &= -(k\phi\,\bar{\psi}_L\psi_R + h.c.) \\ &+ \bar{\psi}\gamma^\mu[q_Y g'_Y A'_{Y\mu} + q_H g_H A'_{H\mu}]\psi, \end{aligned} \tag{10}$$

where g'_Y and g_H are gauge couplings of $\mathrm{U(1)}_Y$ and $\mathrm{U(1)}_H$ in the original basis.

One can make the gauge bosons canonically normalized by the following transformation:

$$A'_{Y\mu} = \frac{A_{Y\mu}}{\sqrt{1-\chi^2}}, \quad A'_{H\mu} = A_{H\mu} - \frac{\chi}{\sqrt{1-\chi^2}}A_{Y\mu}, \tag{11}$$

$$\mathcal{L}_K = -\frac{1}{4}F^{\mu\nu}_Y F_{Y\mu\nu} - \frac{1}{4}F^{\mu\nu}_H F_{H\mu\nu}. \tag{12}$$

Then, in the canonical basis, the gauge interaction terms of ψ are given by

$$\begin{aligned}\bar{\psi}\gamma^\mu(q_Y g'_Y A'_{Y\mu} + q_H g_H A'_{H\mu})\psi = \\ + \bar{\psi}\gamma^\mu[(q_Y - q_{\rm eff})g_Y A_{Y\mu} + q_H g_H A_{H\mu}]\psi,\end{aligned} \tag{13}$$

with

$$g_Y = \frac{g'_Y}{\sqrt{1-\chi^2}}, \quad q_{\rm eff} = q_H \frac{\chi}{\sqrt{1-\chi^2}}\frac{g_H}{g_Y}. \tag{14}$$

One can see that hypercharge gauge coupling g_Y in the canonical basis is larger than g'_Y in the original basis, while g_H remains unchanged under the transformation. Note that the hidden charged particle acquires an effective hypercharge $q_{\rm eff}$ in the canonical basis even if $q_Y = 0$. In this section we set $q_Y = 0$ for simplicity. (In the next section we also consider a case with $q_Y \neq 0$.)

Due to the effective hypercharge, the hidden charged particle also contributes to the electromagnetic anomaly. Its contribution ΔE is

$$\Delta E = \frac{q_H^2 \chi^2}{1-\chi^2}\frac{g_H^2}{g_Y^2} \tag{15}$$

where the right-hand side is evaluated at the mass of ψ, $m_\psi = k v_{PQ}/\sqrt{2}$. Note that $g_{a\gamma\gamma}$ can be significantly enhanced for $\chi = \mathcal{O}(0.1)$ and $q_H g_H = \mathcal{O}(1)$. For instance, we obtain $\Delta E \approx 23$ for $\chi = 0.44$, $q_H g_H = 4.4$ and $g_Y = 0.45$, where those values are motivated by the GUT scenario with $m_\psi = 10^{16}\,\text{GeV}$.

3 Enhanced axion-photon coupling in GUT with $\mathrm{U}(1)_H$

We have shown that $g_{a\gamma\gamma}$ is significantly enhanced if both χ and g_H are large. In fact, such large χ and g_H are strongly favored by the GUT with $\mathrm{U}(1)_H$, as we shall see below. Here and in what follows we consider only complete multiplets under $\mathrm{SU}(5)_{\rm GUT}$.

Firstly, the SM gauge couplings unify at around $M_{\rm GUT} = 10^{16.5}\,\text{GeV}$ with the kinetic mixing of $\chi(m_Z) \approx 0.37$ according to the analysis using the two-loop RGEs [11]. The unification is essentially determined only by $\chi(m_Z)$ and is insensitive to the size of g_H nor the presence of visible and hidden matter fields at an intermediate scale [11, 12].

Secondly, a rather large g_H is required to induce such large kinetic mixing via loop diagrams involving bi-charged fields. To see this, let us introduce N_f bi-charged matter fields, Ψ_{5_i}, which transform as $\mathbf{5}$ under $\mathrm{SU}(5)_{\rm GUT}$ and has $\mathrm{U}(1)_H$ charge of $q_H = -1$. In order for Ψ_{5_i} to induce a large kinetic mixing at the GUT scale, one needs to pick up GUT-breaking effects because of the vanishing sum of hypercharge in the GUT complete multiplets. After the GUT breaking, Ψ_{5_i} generically splits into $\mathrm{SU}(3)_C$ triplet Ψ_{D_i} and $\mathrm{SU}(2)_L$ doublet $\Psi_{\bar{L}_i}$, respectively;

$$-\mathcal{L} \supset \sum_{i=1}^{N_f}\left(M_5 \overline{\Psi}_{5_i}\Psi_{5_i} + k\overline{\Psi}_{5_i}\langle\Sigma_{24}\rangle\Psi_{5_i}\right) = \sum_{i=1}^{N_f}\left(M_D\overline{\Psi}_{D_i}\Psi_{D_i} + M_L\overline{\Psi}_{\bar{L}_i}\Psi_{\bar{L}_i}\right), \tag{16}$$

where $M_5 \sim M_{\rm GUT}$, Σ_{24} is a GUT breaking Higgs, $g_{\rm GUT}$ is a coupling constant of $\mathrm{SU}(5)_{\rm GUT}$, and M_D and M_L are masses of Ψ_{D_i} and $\Psi_{\bar{L}_i}$, respectively. Then, the induced kinetic mixing at one-loop level is estimated as

$$\begin{aligned}\chi(M_{\rm GUT}) &\approx 0.12 N_f \left(\frac{g_{\rm GUT}}{0.53}\right) \\ &\times \left[\frac{g_H(M_{\rm GUT})}{4\pi}\right]\left[\frac{\ln(M_D/M_L)}{\ln 4}\right].\end{aligned} \tag{17}$$

We see that $N_f = \mathcal{O}(1)$ and $g_H(M_{\rm GUT}) \sim 4\pi$ induces the kinetic mixing of $\chi(M_{\rm GUT}) = \mathcal{O}(0.1)$ with a slight mass splitting between M_D and M_L.

With the large χ and g_H motivated by the GUT with $\mathrm{U}(1)_H$, the axion-photon coupling $g_{a\gamma\gamma}$ is significantly enhanced. We consider the following two cases:

$$\begin{aligned}&\text{Case (i)} : \mathcal{L} \supset -\left[\sqrt{2}\phi(\overline{\psi}_{5L}\psi_{5R} + \overline{\psi}_{HL}\psi_{HR}) + h.c.\right], \\ &\text{Case (ii)} : \mathcal{L} \supset -\left[\sqrt{2}\phi\overline{\psi}^{\rm b}_{5L}\psi^{\rm b}_{5R} + h.c.\right],\end{aligned} \tag{18}$$

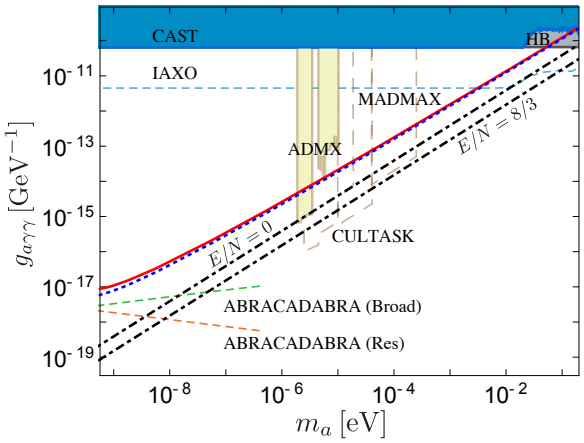

Fig. 1: The predicted axion-photon couplings as a function of the axion mass and experimental constraints. The sensitivity reaches of future experiments are shown as dashed-lines. The figure is taken from Ref. [14].

where ψ_H is a hidden matter field with a charge of $q_H = 1$, which is a SM gauge singlet; $\psi_5(0)$ and $\psi_5^{\rm b}(-1)$ transform as **5** under $\mathrm{SU}(5)_{\rm GUT}$ and their $\mathrm{U}(1)_H$ charges are shown in the parentheses. In Fig 1, we show the predicted $g_{a\gamma\gamma}$ in the cases (i) and (ii), as well as experimental/astrophysical constraints. We take $\chi(m_Z) = 0.365$. The hidden gauge coupling, g_H, is taken as the largest possible value for a fixed f_a, avoiding the Landau pole below the GUT scale. The blue dotted (red solid) line corresponds to the case (i) (case (ii)), where the mass of the matter fields are set to be f_a. Interestingly, some part of the predicted region is already excluded by the ADMX experiment [15, 16], and a large part will be tested by future axion haloscopes such as ADMX [17], CULTASK [18], MADMAX [19], ABRACADABRA [20]. The enhanced $g_{a\gamma\gamma}$ can be also reached by the next generation helioscopes. The sensitivity reach of IAXO [16, 21] is shown as blue-dashed line.

For comparison, the predicted $g_{a\gamma\gamma}$ in the usual case without $\mathrm{U}(1)_H$ are also shown ($E/N = 8/3$ and $E/N = 0$). Here, $E/N = 8/3$ corresponds to the case with $\mathcal{L} \supset -\sqrt{2}\phi(\overline{\psi}_{5L}\psi_{5R} + h.c.)$, which preserves the gauge coupling unification. We see that $g_{a\gamma\gamma}$ in the case (ii) is enhanced by about a factor 10 - 100 for $f_a = 10^{10}$-10^{16} GeV compared to the case of $E/N = 8/3$.

4 Conclusions

We have shown that the axion-photon coupling is enhanced, if the gauge coupling unification is realized by a large kinetic mixing between $\mathrm{U}(1)_Y$ and unbroken hidden $\mathrm{U}(1)_H$. The $\mathrm{U}(1)_H$ gauge coupling should be rather large to induce the large kinetic mixing. Consequently, the axion-photon coupling is enhanced by about a factor 10-100 for $f_a = 10^{10}$-10^{16} GeV, which can be tested in on-going and future experiments.

References

[1] R. D. Peccei and H. R. Quinn, Phys. Rev. Lett. **38**, 1440 (1977).

[2] R. D. Peccei and H. R. Quinn, Phys. Rev. D **16**, 1791 (1977).

[3] S. Weinberg, Phys. Rev. Lett. **40**, 223 (1978).

[4] F. Wilczek, Phys. Rev. Lett. **40**, 279 (1978).

[5] J. Preskill, M. B. Wise and F. Wilczek, Phys. Lett. **120B**, 127 (1983).

[6] L. F. Abbott and P. Sikivie, Phys. Lett. **120B**, 133 (1983).

[7] M. Dine and W. Fischler, Phys. Lett. **120B**, 137 (1983).

[8] P. W. Graham, I. G. Irastorza, S. K. Lamoreaux, A. Lindner and K. A. van Bibber, Ann. Rev. Nucl. Part. Sci. **65**, 485 (2015) [arXiv:1602.00039 [hep-ex]].

[9] I. G. Irastorza and J. Redondo, arXiv:1801.08127 [hep-ph].

[10] J. Redondo, arXiv:0805.3112 [hep-ph].

[11] R. Daido, F. Takahashi and N. Yokozaki, Phys. Lett. B **768**, 30 (2017) [arXiv:1610.00631 [hep-ph]].

[12] F. Takahashi, M. Yamada and N. Yokozaki, Phys. Lett. B **760**, 486 (2016) [arXiv:1604.07145 [hep-ph]].

[13] G. Grilli di Cortona, E. Hardy, J. Pardo Vega and G. Villadoro, JHEP **1601**, 034 (2016) [arXiv:1511.02867 [hep-ph]].

[14] R. Daido, F. Takahashi and N. Yokozaki, Phys. Lett. B **780**, 538 (2018) [arXiv:1801.10344 [hep-ph]].

[15] S. J. Asztalos *et al.* [ADMX Collaboration], Phys. Rev. Lett. **104**, 041301 (2010) [arXiv:0910.5914 [astro-ph.CO]].

[16] G. Carosi, A. Friedland, M. Giannotti, M. J. Pivovaroff, J. Ruz and J. K. Vogel, arXiv:1309.7035 [hep-ph].

[17] S. J. Asztalos *et al.* [ADMX Collaboration], Phys. Rev. D **69**, 011101 (2004) [astro-ph/0310042].

[18] E. Petrakou [CAPP/IBS Collaboration], EPJ Web Conf. **164**, 01012 (2017) [arXiv:1702.03664 [physics.ins-det]].

[19] A. Caldwell *et al.* [MADMAX Working Group], Phys. Rev. Lett. **118**, no. 9, 091801 (2017) [arXiv:1611.05865 [physics.ins-det]].

[20] Y. Kahn, B. R. Safdi and J. Thaler, Phys. Rev. Lett. **117**, no. 14, 141801 (2016) doi:10.1103/PhysRevLett.117.141801 [arXiv:1602.01086 [hep-ph]].

[21] I. G. Irastorza *et al.*, JCAP **1106**, 013 (2011) [arXiv:1103.5334 [hep-ex]].

Extension of the Standard Model by a gauged lepton flavor symmetry and leptogenesis

Kento Asai[a] [1]

[a] *Graduate School of Science, University of Tokyo, 7-3-1 Hongo, Bunkyo-ku, Tokyo, Japan 133-0033*

Abstract

We study the minimal extensions of the Standard Model with three right-handed neutrinos by gauged U(1) lepton flavor symmetries. In some of those models, the mass matrix for the light neutrinos has the so-called two-zero-minor structure, namely, the inverse of the neutrino mass matrix has two vanishing components. Analyzing these conditions, we obtain all the CP phases, such as the Dirac CP phase δ and the Majorana CP phases α_2 and α_3, and the mass eigenvalues of the light neutrinos m_i as functions of the neutrino mixing angles θ_{12}, θ_{23}, and θ_{13}, and the squared mass differences Δm^2_{21} and Δm^2_{31}. Furthermore, using these results, we also obtain the predictions for the sum of the neutrino masses $\Sigma_i m_i$ and the effective neutrino mass $\langle m_{\beta\beta}\rangle$. In addition, we also discuss the implication of our results for leptogenesis. Because space is limited, in this report, we show a part of our work.

1 Introduction

A gauged U(1) lepton flavor symmetry is one of the possibilities of extension of the Standard Model (SM) and it is known that $\mathrm{U}(1)_{L_i-L_j}$ gauge symmetries, where L_i represents the lepton number of generation associated with i $(= e, \mu, \tau)$, can be introduced without anomalies. We focus on the cases where the neutrino mass matrix has the so-called two-zero-minor structure, namely, the inverse of them has two vainishing components. In Ref. [1], the relation between gauged U(1) lepton flavor symmetries and structures of the neutrino mass matrix was comprehensively discussed. In the case of the minimal extended model by a $\mathrm{U}(1)_{L_\mu-L_\tau}$ gauge symmetry, we discussed the relation between two-zero-minor conditions and the neutrino parameters, such as the CP phases, the neutrino masses, and the effective neutrino mass, and gave the predictions for them in Ref. [2].

In the workshop, we presented results of the study [3], where we extended extra U(1) gauge symmetries to ones obtained as a linear combination of the $\mathrm{U}_{L_e-L_\mu}$, $\mathrm{U}(1)_{L_\mu-L_\tau}$, and $\mathrm{U}(1)_{B-L}$ gauge symmetries. Then, we discussed that relation as we have done in Ref. [2] and, in the case of the five U(1) gauge symmetries that were consistent with the resent neutrino oscillation data, we obtained all the CP phases, such as the Dirac CP phase δ and the Majorana CP phases α_2 and α_3, and the mass eigenstates of the light neutrinos as functions of the neutrino mixing angles θ_{12}, θ_{23}, and θ_{13}, and the squared mass differences Δm^2_{21} and Δm^2_{31}. We also discussed the implication of our results for leptogenesis. However, since space is limited, we show only the derivation of the two-zero-minor conditions and the prediction for the sum of the neutrino masses in this report.[2]

2 Analyses of neutrino mass structure

Because of the anomaly-free condition, allowed linear combination of gauged U(1) lepton flavor symmetries are $\mathrm{U}(1)_{aL_e+bL_\mu-(a+b)L_\tau}$ and $\mathrm{U}(1)_{B+aL_e+bL_\mu+(3-a-b)L_\tau}$, where a and b are real

[1] asai@hep-th.phys.s.u-tokyo.ac.jp

[2] The details are written in Ref. [3].

numbers. To avoid verbose description, however, we consider only the $U(1)_{L_\mu - L_\tau}$ case and analyze the neutrino mass matrix following Ref [2]. In the case of other U(1) symmetries, we can use the same method. In the minimal gauged $U(1)_{L_\mu - L_\tau}$ model, the interaction terms relevant to neutrino masses are given by

$$\begin{aligned}\Delta\mathcal{L} = &- \lambda_e N_e^c (L_e \cdot H) - \lambda_\mu N_\mu^c (L_\mu \cdot H) - \lambda_\tau N_\tau^c (L_\tau \cdot H) \\ &- \frac{1}{2} M_{ee} N_e^c N_e^c - M_{\mu\tau} N_\mu^c N_\tau^c - \lambda_{e\mu} \sigma N_e^c N_\mu^c - \lambda_{e\tau} \sigma^* N_e^c N_\tau^c + \text{h.c.} \ , \end{aligned} \tag{1}$$

where the dots indicate the contraction of the $SU(2)_L$ indices. After the Higgs field H and the singlet scalar σ acquire VEVs $\langle H \rangle = v/\sqrt{2}$ and $\langle \sigma \rangle$,[3] the Dirac and Majorana mass matrices are obtained as follows:

$$\mathcal{M}_D = \frac{v}{\sqrt{2}} \begin{pmatrix} \lambda_e & 0 & 0 \\ 0 & \lambda_\mu & 0 \\ 0 & 0 & \lambda_\tau \end{pmatrix} \ , \qquad \mathcal{M}_R = \begin{pmatrix} M_{ee} & \lambda_{e\mu}\langle\sigma\rangle & \lambda_{e\tau}\langle\sigma\rangle \\ \lambda_{e\mu}\langle\sigma\rangle & 0 & M_{\mu\tau} \\ \lambda_{e\tau}\langle\sigma\rangle & M_{\mu\tau} & 0 \end{pmatrix} \ . \tag{2}$$

The mass matrix for the light neutrinos is given by [4]

$$\mathcal{M}_{\nu_L} \simeq -\mathcal{M}_D \mathcal{M}_R^{-1} \mathcal{M}_D^T \ . \tag{3}$$

We can obtain the mass eigenvalues of the light neutrinos by diagonalizing this matrix using a unitary matrix U (PMNS matrix [4] [5]):

$$U^T \mathcal{M}_{\nu_L} U = \text{diag}(m_1, m_2, m_3) \ . \tag{4}$$

In this report, we consider only the $m_i \neq 0$ cases. For if $m_i = 0$ ($i = 1$ or 3), the mass matrix for the light neutrinos $\mathcal{M}_{\nu_L}$ is block-diagonal, and we cannot have desired mixing angles. From Eqs. (3) and (4),

$$\mathcal{M}_{\nu_L}^{-1} = U \text{diag}(m_1^{-1}, m_2^{-1}, m_3^{-1}) U^T \simeq -(\mathcal{M}_D^{-1})^T \mathcal{M}_R \mathcal{M}_D^{-1} \ . \tag{5}$$

In this model, $\mathcal{M}_D$ is diagonal and (μ, μ) and (τ, τ) components in $\mathcal{M}_R$ vanish, so these components in the inverse of $\mathcal{M}_{\nu_L}$ also have to vanish. These two conditions, which these components in $\mathcal{M}_{\nu_L}^{-1}$ have to satisfy, are given by

$$\frac{1}{m_1} V_{\mu 1}^2 + \frac{1}{m_2} V_{\mu 2}^2 \, e^{i\alpha_2} + \frac{1}{m_3} V_{\mu 3}^2 \, e^{i\alpha_3} = 0 \ , \tag{6}$$

$$\frac{1}{m_1} V_{\tau 1}^2 + \frac{1}{m_2} V_{\tau 2}^2 \, e^{i\alpha_2} + \frac{1}{m_3} V_{\tau 3}^2 \, e^{i\alpha_3} = 0 \ , \tag{7}$$

where the matrix V is defined by $U = V \cdot \text{diag}(1, e^{i\alpha_2/2}, e^{i\alpha_3/2})$. We notice that neither the $U(1)_{L_\mu - L_\tau}$-breaking singlet VEV $\langle\sigma\rangle$ nor Majorana masses M_{ee} and $M_{\mu\tau}$ appear in these conditions explicitly, and so the following discussions and results based on the above conditions are independent of these scales. Eqs. (6) and (7) are two complex equations, therefore, by solving these equations, we can obtain the Dirac CP phase δ, the Majorana CP phases $\alpha_{2,3}$, and the mass eigenvalue of the lightest neutrino m_1, as functions of the mixing angles θ_{12}, θ_{23}, and θ_{13}, and the squared mass differences Δm_{21}^2 and Δm_{32}^2. [5]

[3] We can always take the VEV of σ to be real by using $U(1)_{L_\mu - L_\tau}$ transformations.

[4] We follow the convention of the Particle Data Group [6].

[5] For concrete calculations and explicit expressions, see Ref [2].

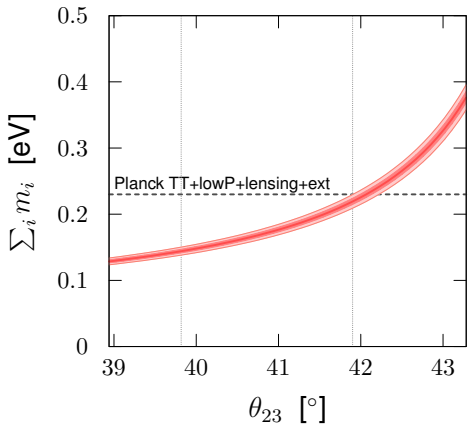

Figure 1: The prediction for the sum of the neutrino masses as a function of θ_{23}. The dark (light) red band shows the uncertainty coming from the 1σ (2σ) errors in the parameters θ_{12}, θ_{13}, δm^2, and Δm^2. The entire region is within the 2σ range of θ_{23}, while its 1σ range is between the thin vertical dotted lines. We also show in the black dashed line the present limit imposed by the Planck experiment: $\sum_i m_i < 0.23$ eV (Planck TT+lowP+lensing+ext) [7].

Since space is limited, we show only the prediction for the sum of the neutrino masses as a function of θ_{23} in Fig. 1, where the dark (light) red band shows the uncertainty coming from the 1σ (2σ) errors in the parameters other than θ_{23}. We also show in the black dashed line the present limit imposed by the Planck experiment: $\Sigma_i m_i < 0.23$ eV (Planck TT+lowP+lensing+ext) [7]. From this figure, we find that a wide range of the parameter region predicts a value of $\Sigma_i m_i$ which is below the present limit, though a part of the parameter region has already been disfavored by the Planck limit.

Acknowledgement

KA is supported by the Program for Leading Graduate Schools, MEXT, Japan.

References

[1] T. Araki, J. Heeck, and J. Kubo, JHEP **07** (2012) 083.

[2] K. Asai, K. Hamaguchi, and N. Nagata, Eur. Phys. J. **C77** (2017) no.11 763.

[3] K. Asai, Mater's thesis (Unpublished), Univ. of Tokyo (2018); K. Asai, K. Hamaguchi, and N. Nagata (in preparation).

[4] P. Minkowski, Phys. Lett. **B67** (1977) 421-428; T. Yanagida, Conf. Proc. **C7902131** (1979) 95-99; M. Gell-Mann, P. Ramond, and R. Slansky, Conf. Proc. **C790927** (1979) 315-321; R. N. Mohapatra and G. Senjanovic, Phys. Rev. Lett. **44** (1980) 912.

[5] B. Pontecorvo, Sov. Phys. JETP **7** (1958) 172-173. [Zh. Eksp. Teor. Fiz. **34** (1957) 247]; Z. Maki, M. Nakagawa, and S. Sakata, Prog. Theor. Phys. **28** (1962) 870-880.

[6] **Particle Data Group** Collaboration, C. Patrignani et al., Chin. Phys. **C40** (2016), no. 10 100001.

[7] **Planck** Collaboration, P. A. R. Ade et al., Astron. Astrophys. **594** (2016) A13.

CPT violation in neutrinos

Gabriela Barenboim*
Departament de Física Teòrica and IFIC, Universitat de València-CSIC, E-46100, Burjassot, Spain
(Dated: March 7, 2019)

CPT symmetry, the combination of Charge Conjugation, Parity and Time reversal, is a cornerstone of our model building strategy and therefore the repercussions of its potential violation will severely threaten the most extended tool we currently use to describe physics, *i.e.* local relativistic quantum fields. However, limits on its conservation from the Kaon system look indeed imposing. In this talk I will show that neutrino oscillation experiments can improve this limit by several orders of magnitude and therefore are an ideal tool to explore the foundations of our approach to Nature.

Striclty speaking testing CPT violation would require an explicit model for how CPT is broken and its effects on physics. Instead, what is presented in this work is a test of one of the predictions of CPT conservation, ie, the same mass and mixing parameters in neutrinos and anti-neutrinos. In order to do that we calculate the current CPT bound on all the neutrino mixing parameters.

After deriving the most updated bound on CPT from neutrino oscillation data, I will show that, if the recent T2K results turn out to be the true values of neutrino and antineutrino oscillations, DUNE would measure the fallout of CPT conservation at more than 3σ. Finally I show that, if CPT is violated in nature, combining neutrino with antineutrino data in oscillation analysis will produce imposter solutions.

INTRODUCTION

CPT invariance is surely one of the predictions of major importance of local, relativistic quantum field theory. One of the predictions of CPT invariance is that particles and antiparticles have the same masses and, if unstable, the same lifetimes. To prove the CPT theorem one needs only three ingredients [1]:

1. Lorentz invariance
2. Hermiticity of the Hamiltonian
3. Locality

If CPT turned out to be violated, the effect on modern fundamental particle physics would be gigantic. We would have to rethink our model-building strategies, since one of the three ingredients above would not hold anymore. Experimental bounds on CPT invariance can be derived using the neutral kaon system [2]:

$$\frac{|m(K^0) - m(\overline{K}^0)|}{m_K} < 0.6 \times 10^{-18}\,. \tag{1}$$

This result, however, should be interpreted very carefully because of two reasons: first, we do not have a complete theory of CPT violation. Therefore, it is rather arbitrary to take the kaon-mass as a scale. Second, since kaons are bosons, the term entering the Lagrangian is the mass squared and not the mass itself. Having this in mind, we can rewrite the previous bound in this way

$$|m^2(K^0) - m^2(\overline{K}^0)| < 0.25 \text{ eV}^2\,. \tag{2}$$

Here we will see that neutrinos can test the predictions of the CPT theorem to an unprecedented extent and could therefore provide stronger limits than the ones regarded as the most stringent ones by now, It should be noticed that CPT was tested also using charged leptons. However, these measurements involve a combination of mass and charge and are not a direct CPT test. Only neutrinos can provide CPT tests on an elementary mass not contaminated by charge.. In the absence of a solid model of flavor, not to mention one of CPT violation, the spectrum of neutrinos and antineutrinos can differ both in the mass eigenstates themselves as well as in the flavour composition of each of these states. It is important to notice then that neutrino oscillation experiments can only test CPT in the mass differences and mixing angles. An overall shift between the neutrino and antineutrino spectra will be missed by oscillation experiments. Nevertheless such a pattern can be bounded by cosmological data, see Ref. [3]. Unfortunately direct searches for neutrino mass (past, present and future) involve only antineutrinos and therefore cannot be used to draw any conclusion on CPT invariance on the absolute mass scale either. Therefore, using neutrino oscillation data, we will compare the mass splittings and mixing angles of neutrinos with those of antineutrinos. Differences in the neutrino and antineutrino spectrum, as schematically depicted in Fig. 1, would imply the violation of the CPT theorem. Let us stress, however, that without an explicit model for CPT violation [4] it is not straightforward or even meaningful to compare the neutrino-antineutrino mass squared differences and the kaon ones. CPT violation may show up only in one of the sectors and therefore the strong bounds in one of them might not be directly applicable to the other. Nevertheless, there are reasons to believe that neutrinos are an ideal candidate to test CPT violation: quantum gravity is assumed to be non-local, opening the door to a potential CPT violation. Its effects, however, are expected to be Planck suppressed, *i.e.* $\langle v \rangle^2 / M_{\rm P}$, exactly in the right ballpark for neutrino experiments to

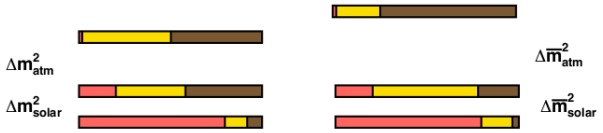

FIG. 1: Generic CPT violating spectrum. We have not included an overall shift between the neutrino and antineutrino sector as it cannot be tested by oscillation experiments

see them. Also, since neutrinos offer a unique mass generation mechanism, the see-saw, their masses should be sensitive to new physics and new scales. Scales where non-locality might show up.

In Ref. [6] the authors derived most up-to-date bounds on CPT invariance from the neutrino sector. The data used to derive these bounds are the same considered in the global fit to neutrino oscillations in Ref. [7]. Of course, experiments which cannot distinguish between neutrinos and antineutrinos, such as atmospheric data from Super-Kamiokande, IceCube-DeepCore and ANTARES were not included. The complete data set used, as well as the parameters they are sensitive to are the following:

- solar neutrino data: θ_{12}, Δm^2_{21}, θ_{13}
- neutrino mode in long–baseline experiments K2K, MINOS, T2K and NOνA: θ_{23}, Δm^2_{31}, θ_{13}
- KamLAND reactor antineutrino data: $\overline{\theta}_{12}$, $\Delta\overline{m}^2_{21}$, $\overline{\theta}_{13}$
- short–baseline reactor antineutrino experiments Daya Bay, RENO and Double Chooz: $\overline{\theta}_{13}$, $\Delta\overline{m}^2_{31}$
- antineutrino mode in long–baseline experiments (The K2K experiment took data only in neutrino mode, while the NOνA experiment has not published data in the antineutrino mode yet) MINOS and T2K: $\overline{\theta}_{23}$, $\Delta\overline{m}^2_{31}$ $\overline{\theta}_{13}$

From the analysis of all previous data samples, one can derive the most up-to-date bounds on CPT violation:

$$\begin{aligned} |\Delta m^2_{21} - \Delta\overline{m}^2_{21}| &< 4.7\times10^{-5}\,\mathrm{eV}^2, \\ |\Delta m^2_{31} - \Delta\overline{m}^2_{31}| &< 3.7\times10^{-4}\,\mathrm{eV}^2, \\ |\sin^2\theta_{12} - \sin^2\overline{\theta}_{12}| &< 0.14, \\ |\sin^2\theta_{13} - \sin^2\overline{\theta}_{13}| &< 0.03, \\ |\sin^2\theta_{23} - \sin^2\overline{\theta}_{23}| &< 0.32. \end{aligned} \tag{3}$$

At the moment it is not possible to set any bound on $|\delta - \overline{\delta}|$, since all possible values of δ or $\overline{\delta}$ are allowed by data. The preferred intervals of δ obtained in Ref. [7] can only be obtained after combining the neutrino and antineutrino data samples. The limits on $\Delta(\Delta m^2_{31})$ and $\Delta(\Delta m^2_{21})$ are already better than the one derived from the neutral kaon system and should be regarded as the best bounds on CPT violation on the mass squared so far.

Regarding the future, the Deep Underground Neutrino Experiment (DUNE) will consist of two detectors exposed to a megawatt-scale muon neutrino beam that will be produced at Fermilab. DUNE will be using 1.47×10^{21} protons on target (POT) per year, which amounts basically in one single year to the same amount T2K has used in all of its lifetime until now (runs 1–7c). Performing the CPT violating analysis with DUNE setup we obtain very interesting results for $\Delta(\Delta m^2_{31})$ and $\Delta(\sin^2\theta_{23})$. We find that DUNE should be able to set bounds on $\Delta(\Delta m^2_{31})$ tighter than 8.1×10^{-5} at 3σ confidence level. This would imply an improvement of one order of magnitude with respect to the old bound and four orders of magnitude with respect to the neutral Kaon bound, once it is viewed as a bound on the mass squared. Concerning the atmospheric mixing angle, we obtain different results depending on the true value assumed to simulate DUNE data. In the case of true maximal mixing, the sensitivity increases with $\Delta(\sin^2\theta_{23})$, as one might expect. However, if we assume the true values to be in the first or second octant, a degenerate solution appears in the complementary octant.

In different types of neutrino oscillation experiments, as for example accelerators, neutrino and antineutrino data are obtained in separate experimental runs. However, the usual procedure followed by the experimental collaborations, as well as the global oscillation fits as for example Ref. [7], assumes CPT invariance and analyzes the full data sample in a joint way. Such a path is not risk-free. Indeed, the opportunity to test CPT invariance in the neutrino sector is lost. Even more important, if CPT is violated in nature, the outcome of the joint data analysis might give rise to what we call an imposter solution. A solution which results from the combined analysis but does not correspond to the true solution of any channel.

Under the assumption of CPT conservation, the χ^2–functions are computed according to

$$\chi^2_{\mathrm{total}} = \chi^2(\nu) + \chi^2(\overline{\nu})\,, \tag{4}$$

and assuming that the same parameters describe neutrino and antineutrino flavor oscillations. In contrast, in our analysis we first marginalized over the parameters in neutrino and antineutrino mode separately and then added the marginalized profiles. Here, we shall assume CPT to be violated in nature, but perform our analysis as if it was conserved. As an example, we assume

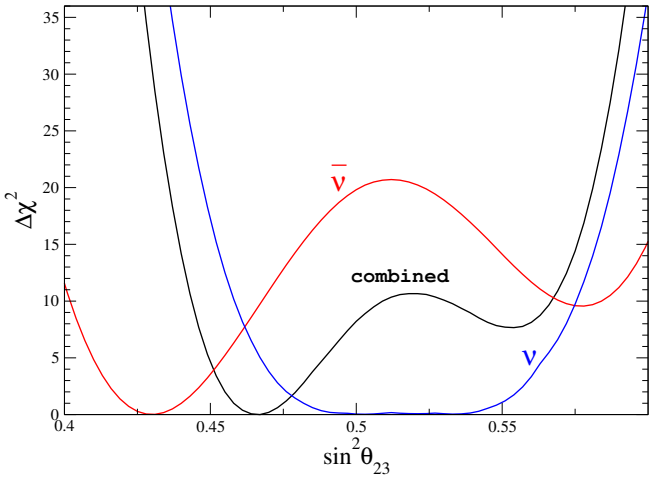

FIG. 2: DUNE sensitivity to the atmospheric angle for neutrinos (blue), antineutrinos (red) and to the combination of both under the assumption of CPT conservation (black).

that the true value for the atmospheric neutrino mixing is $\sin^2\theta_{23} = 0.5$, while the antineutrino mixing angle is given by $\sin^2\overline{\theta}_{23} = 0.43$. The rest of the oscillation parameters are set to their best fit values. Performing the statistical analysis in the CPT conserving way, as indicated in Eq. (4), we obtain the profile of the atmospheric mixing angle presented in Fig. 2. The profiles for the individual reconstructed results (neutrino and antineutrino) are also shown in the figure for comparison. As can be seen, we obtain a new best fit value at $\sin^2\theta_{23}^{\rm comb} = 0.467$, disfavoring the true values for neutrino and antineutrino parameters at approximately 3σ and more than 5σ, respectively.

ACKNOWLEDGEMENTS

GB acknowledges support from the MEC and FEDER (EC) Grants SEV-2014-0398 FIS2015-72245-EXP and FPA-2017-84543P and the Generalitat Valenciana under grant PROMETEOII/2013/017.

* Gabriela.Barenboim@uv.es

[1] R. F. Streater and A. S. Wightman, Princeton, USA: Princeton Univ. Pr. (2000) 207 p.
[2] B. Schwingenheuer *et al.*, Phys. Rev. Lett. **74**, 4376 (1995). doi:10.1103/PhysRevLett.74.4376
[3] G. Barenboim and J. Salvado, Eur. Phys. J. C **77**, no. 11, 766 (2017) doi:10.1140/epjc/s10052-017-5347-y [arXiv:1707.08155 [hep-ph]].
[4] G. Barenboim and J. D. Lykken, Phys. Lett. B **554**, 73 (2003) doi:10.1016/S0370-2693(02)03262-8 [hep-ph/0210411].
[5] G. Barenboim, C. A. Ternes and M. Trtola, arXiv:1804.05842 [hep-ph].
[6] G. Barenboim, C. A. Ternes and M. Trtola, Phys. Lett. B **780**, 631 (2018) doi:10.1016/j.physletb.2018.03.060 [arXiv:1712.01714 [hep-ph]].
[7] P. F. de Salas, D. V. Forero, C. A. Ternes, M. Tortola and J. W. F. Valle, arXiv:1708.01186 [hep-ph].

Acknowledgement PPAP2018 is supported JSPS Grant-in Aid for Scientific Research (C) Grant Number JP17K05418 (Takuya Morozumi) and Core of Research for the Energetic Universe (Core-U) of Hiroshima University. We thank Midori Maeda and all the members of Particle Physics Group of Hiroshima University for their help and encouragement. All the slides of talks can be found in https://home.hiroshima-u.ac.jp/morozumi/ppapo.html.